Adaptive isogeometric methods with C^1 (truncated) hierarchical splines on planar multi-patch domains

Cesare Bracco[1], Carlotta Giannelli[1], Mario Kapl[2], R. Vázquez[3,4]

[1] Dipartimento di Matematica e Informatica "U. Dini", Università degli Studi di Firenze, Florence, Italy

[2] Department of Engineering & IT, Carinthia University of Applied Sciences, Villach, Austria

[3] Institute of Mathematics, École Polytechnique Fédérale de Lausanne, Lausanne, Switzerland

[4] Istituto di Matematica Applicata e Tecnologie Informatiche 'E. Magenes' del CNR, Pavia, Italy

April 21, 2022

Abstract

Isogeometric analysis is a powerful paradigm which exploits the high smoothness of splines for the numerical solution of high order partial differential equations. However, the tensor-product structure of standard multivariate B-spline models is not well suited for the representation of complex geometries, and to maintain high continuity on general domains special constructions on multi-patch geometries must be used. In this paper we focus on adaptive isogeometric methods with hierarchical splines, and extend the construction of C^1 isogeometric spline spaces on multi-patch planar domains to the hierarchical setting. We introduce a new abstract framework for the definition of hierarchical splines, which replaces the hypothesis of local linear independence for the basis of each level by a weaker assumption. We also develop a refinement algorithm that guarantees that the assumption is fulfilled by C^1 splines on certain suitably graded hierarchical multi-patch mesh configurations, and prove that it has linear complexity. The performance of the adaptive method is tested by solving the Poisson and the biharmonic problems.

Keywords: Isogeometric analysis; Adaptivity; Hierarchical splines; C^1 continuity; Multi-patch domains; Biharmonic problem

AMS Subject Classification: 65D07; 65D17; 65N30; 65N50

1 Introduction

Isogeometric Analysis (IgA) is a numerical method for the solution of partial differential equations (PDEs), introduced with the idea of bridging the gap between computer aided design and finite element analysis. The fundamental idea is the use of (rational) spline functions both for the representation of the geometry and for the discretization of the PDEs, allowing a simpler interaction between them. It was very soon realized that one of the main advantages of IgA is the high continuity of splines, which is particularly useful in the solution of high order PDEs such as the stream formulation of linear elasticity [3], the Kirchhoff-Love shell [43] or the Cahn-Hilliard phase field model [27], because they allow a straightforward discretization of their direct formulations, that require the basis functions to be C^1, or more precisely, H^2-conforming.

The high continuity of the basis functions is trivially obtained in a single-patch representation of the domain, but the design of complex geometry models requires the use of a globally unstructured representation as the one given by multi-patch domains. While C^0 continuity across patches is relatively easy to obtain, as long as the meshes are conforming on the interfaces, the construction of isogeometric C^1 spline functions on complex multi-patch domains is more challenging, and has been extensively studied in recent years. The existing methods can be classified into two groups depending on whether the C^1 continuity of the spline spaces is exact or just approximate. In case of approximately C^1 multi-patch spline spaces, possible examples are methods which enforce the C^1-smoothness across the interfaces weakly, e.g. by adding penalty

terms to the weak form of the PDE as in [2, 29] or by means of Lagrange multipliers as in [2, 5], and methods which approximate the C^1 continuity directly on the basis functions as in [50, 53, 58, 59]. In case of exactly C^1 multi-patch spline spaces, the methods can be distinguished depending on the employed parameterization of the multi-patch domain. Examples are the use of multi-patch parameterizations which are C^1 everywhere and therefore possessing singularities at extraordinary vertices such as in [48, 54] or in subdivision based techniques [46, 49, 60], non-singular multi-patch geometries which are C^1 everywhere except in the neighborhood of extraordinary vertices where a G^1-cap is used [40, 41, 42, 47] as well as non-singular multi-patch parameterizations which are in general just G^1 at all interfaces (or in case of planar domains even just C^0). In the latter case, examples are approaches based on arbitrary topology meshes with specific piecewise polynomial patches [8, 9, 45], methods employing generic spline patches [18, 19] or techniques using analysis-suitable (AS) G^1 multi-patch parameterizations [20]. For more exhaustive explanations about the construction of globally C^1 spline spaces we refer to the two recent survey articles [32, 36].

In this paper we will consider analysis-suitable (AS) G^1 multi-patch parameterizations, which contain the subset of (mapped) piecewise bilinear domains [6, 33, 38] as special case. Their use, however, is not particularly restrictive because generic multi-patch parameterizations can be usually reparameterized to be AS G^1 [35]. The importance of analysis-suitable G^1 geometries is that they allow the construction of C^1 multi-patch spline spaces with optimal polynomial reproduction properties, and therefore isogeometric methods based on those spaces have optimal convergence, as numerically shown in [36, 37]. In particular, our focus will be on the addition of local refinement capabilities to the C^1 spline space from [37], since (1) it has a simple and explicitly given local basis, (2) its dimension is independent of the parameterizations of the single patches, and (3) the number of basis functions associated to each extraordinary vertex is equal to six independently of the vertex valence.

The main advantage of adaptive isogeometric methods is that they provide the possibility to locally refine the approximation space of the considered PDE, which allows in general to attain the same accuracy as global refinement with an important reduction in the degrees of freedom and the computational effort. Among all the possible spline spaces with local refinement capabilities, we here focus on (truncated) hierarchical splines [25, 24], because their multilevel structure simplifies their use with respect to other spline spaces, see [13, Chapter 4] for a discussion on the use of adaptive spline spaces in isogeometric analysis. The theoretical background of adaptive methods with hierarchical B-splines in IgA was investigated in [14, 15, 22], where the optimal convergence rates for second order elliptic PDEs was proved. The potential benefits of adaptivity with hierarchical splines for the solution of fourth order PDEs were studied to simulate brittle fracture in [31, 30], for Kirchhoff plates and Kirchhoff-Love shells in [1, 21], and for the simulation of tumor growth in [44], always restricted to the case of single-patch domains.

The use of C^1 multi-patch spaces with local refinement was initiated with works on T-splines, as in [51, 57] and references therein, and subdivision surfaces [56], but the approximation properties of the spaces were not optimal around extraordinary points. In the last years, the construction of C^1 splines based on degenerate patches (also called D-patches) from [54] improved the accuracy around extraordinary vertices with respect to previous works, and it was extended from uniform refinement to T-splines in [17], and very recently to hierarchical splines in [55], although the properties required for the hierarchical construction were only studied numerically. The construction based on the C^1 space of [37] was extended to hierarchical splines in [11] for two-patch geometries, that is, in the absence of extraordinary points.

In this work we generalize the construction of C^1 hierarchical splines from the two-patch to the multi-patch setting. Since the presence of extraordinary points removes the local linear independence property, usually considered so far for the construction of hierarchical spline spaces, our first contribution is the development of a new hierarchical spline setting, which only assumes a decomposition of the basis of each level into subsets with suitable linear independence conditions on selected regions. We prove that this relaxed assumption implies linear independence of the (truncated) hierarchical basis. Second, we present the characterization of the C^1 space on one level, as well as a counterexample of the local linear independence of its basis and key results about linear independence of certain basis subsets. Third, relying on these properties we construct the new hierarchical C^1 spline space, with an explicit expression of the refinement mask necessary to apply truncation. We show that under a simple condition on the hierarchical mesh near the extraordinary point the assumptions of the new framework are satisfied, and we develop a simple refinement algorithm to ensure

that this condition is always satisfied. In practice, whenever an element adjacent to an extraordinary vertex is marked for refinement, other elements of the same patch (at most four) must be also marked. Fourth, we combine the new algorithm with admissible refinement algorithms from [12] and [14] to limit the interaction between functions of different levels, and prove its linear complexity. Finally, we show numerical evidence for the optimal convergence properties of the proposed adaptive scheme for different model problems.

The remainder of the paper is organized as follows. Section 2 presents the new abstract framework for the definition of (truncated) hierarchical splines. In Section 3 we introduce all the necessary material regarding analysis-suitable G^1 multi-patch parameterizations and the considered C^1 spline space, with additional information detailed in A. Section 4 investigates the properties of the one level C^1 multi-patch space, while Section 5 introduces the construction of the C^1 hierarchical spline space. We further present in this section a refinement algorithm that ensures the property of linear independence and admissibility, and show the linear complexity of the algorithm. In Section 6, we demonstrate the potential of our novel adaptive method for applications in IgA by solving the Poisson and the biharmonic problems over different AS-G^1 multi-patch geometries, and we give some conclusions in Section 7.

2 New abstract framework for hierarchical spline spaces

This section introduces an abstract framework for the construction of the hierarchical spline basis, which relaxes the assumption of *local linear independence* for the underlying sequence of spline bases, as originally considered in [26] and also assumed in the construction of C^1 hierarchical functions on two-patch geometries [11].

2.1 Hierarchical splines

Let $\mathbb{U}^0 \subset \mathbb{U}^1 \subset \ldots \subset \mathbb{U}^{N-1}$ be a sequence of nested multivariate spline spaces defined on the closed domain $D \subset \mathbb{R}^d$ and let

$$\Omega^0 \supseteq \Omega^1 \supset \ldots \supset \Omega^{N-1}$$

be a sequence of closed nested domains with $\Omega^0 \subseteq D$. We assume that any space $\mathbb{U}^\ell$, for $\ell = 0, \ldots, N-1$, is spanned by the basis Ψ^ℓ, which can be decomposed as

$$\Psi^\ell := \bigcup_{i \in I^\ell} \Psi_i^\ell,$$

satisfying the following properties:

(P1) for each level ℓ and $i \in I^\ell$ there exists $D_i^\ell \subseteq \Omega^\ell \setminus \Omega^{\ell+1}$ where Ψ_i^ℓ is linearly independent and

$$\operatorname{span} \Psi_i^\ell \cap \operatorname{span} \widetilde{\Psi}_i^\ell = \{0\},$$

with $\widetilde{\Psi}_i^\ell := \Psi^\ell \setminus \Psi_i^\ell$;

(P2) local and compact support.

The second property localizes the influence of the basis functions and is directly exploited in the definition of the hierarchical spline basis $\mathcal{H}$ as follows:

$$\mathcal{H} := \left\{ \psi \in \Psi^\ell : \operatorname{supp}^0 \psi \subseteq \Omega^\ell \wedge \operatorname{supp}^0 \psi \not\subseteq \Omega^{\ell+1}, \ell = 0, \ldots, N-1 \right\}, \tag{1}$$

where $\operatorname{supp}^0 \psi := \operatorname{supp} \psi \cap \Omega^0$. The first property, instead, is used to prove the linear independence of the hierarchical basis in the following theorem. Note that if the basis Ψ^ℓ satisfies the property of local linear independence, then property (P1) trivially holds without any decomposition by always taking $D^\ell = \Omega^\ell \setminus \Omega^{\ell+1}$.

Theorem 2.1. *By assuming that property (P1) holds for the basis Ψ^ℓ, for $\ell = 0, \ldots, N-1$, the hierarchical spline basis $\mathcal{H}$ is linearly independent.*

Proof. The sum

$$\sum_{\psi\in\mathcal{H}} c_\psi\psi = \sum_{\ell=0}^{N-1}\left(\sum_{i\in I^\ell}\left(\sum_{\psi\in\Psi_i^\ell\cap\mathcal{H}} c_\psi\psi\right)\right) = 0$$

can be obviously written as

$$\sum_{i\in I^0}\left(\sum_{\psi\in\Psi_i^0\cap\mathcal{H}} c_\psi\psi\right) + \sum_{i\in I^1}\left(\sum_{\psi_i\in\Psi_i^1\cap\mathcal{H}} c_\psi\psi\right) + \ldots + \sum_{i\in I^{N-1}}\left(\sum_{\psi_i\in\Psi_i^{N-1}\cap\mathcal{H}} c_\psi\psi\right) = 0.$$

In virtue of the definition of the hierarchical spline basis (1), the basis functions collected by the first sum in the expression above are the only nonzero functions acting on the region given by $\Omega^0 \setminus \Omega^1$. Property (P1) guarantees that for each $i \in I^0$ there exists $D_i^0 \subseteq \Omega^0 \setminus \Omega^1$ where Ψ_i^0 is linearly independent and its span has null intersection with the span of any other subset of basis functions Ψ_j^0 with $j \neq i$ except for the zero constant. Consequently, the corresponding coefficients c_ψ must be zero for any $\psi \in \Psi_i^0$, $i \in I^0$.

For any level $\ell = 1, \ldots, N-1$, excluding the functions already considered in the sums of previous levels $\tilde{\ell} = 0, \ldots, \ell-1$, the basis functions collected by the sum of level ℓ are the only nonzero functions which act on $\Omega^\ell \setminus \Omega^{\ell+1}$. By iteratively exploiting (P1), we can then proceed with the same argument considered for $\ell = 0$ and conclude that the coefficient c_ψ associated to any $\psi \in \Psi_i^\ell$ with $i \in I^\ell$ must be zero. □

2.2 Truncated hierarchical splines

Replacing the property of local linear independence with property (P1) still allows us to define the truncated hierarchical basis, as originally introduced for hierarchical B-splines in [25] and later analyzed in a more general setting in [26]. In fact, in view of the nested nature of the sequence of spline spaces $(\mathbb{U}^\ell)_{\ell=0,\ldots,N-1}$, we can exploit a two-scale relation between bases of consecutive hierarchical levels to express any spline s in the spline space of level ℓ ($\operatorname{span}\Psi^\ell$) as a linear combination of basis functions in $\Psi^{\ell+1}$, namely

$$s = \sum_{\psi\in\Psi^{\ell+1}} c_\psi^{\ell+1}(s)\psi, \tag{2}$$

and to define the truncation of s at level $\ell+1$ as

$$\operatorname{trunc}^{\ell+1}(s) := \sum_{\psi\in\Psi^{\ell+1},\, \operatorname{supp}^0\psi\not\subseteq\Omega^{\ell+1}} c_\psi^{\ell+1}(s)\psi.$$

The truncated hierarchical basis is then given by

$$\mathcal{T} := \left\{\operatorname{Trunc}^{\ell+1}(\psi) : \psi\in\Psi^\ell\cap\mathcal{H}, \ell = 0,\ldots,N-1\right\}, \tag{3}$$

where

$$\operatorname{Trunc}^{\ell+1}(\psi) := \operatorname{trunc}^{N-1}\left(\ldots\left(\operatorname{trunc}^{\ell+1}(\psi)\right)\ldots\right) \tag{4}$$

defines the successive truncation of the basis function ψ of level ℓ, for $\ell = 0,\ldots,N-2$, and $\operatorname{Trunc}^N(\psi) = \psi$ for any $\psi \in \Psi^{N-1}$. Any hierarchical basis function $\psi \in \mathcal{H}$ generates a truncated basis function $\tau \in \mathcal{T}$ according to (4) and it is called the mother function of the child function τ, and (as in the setting of [26]) for the two functions it holds that

$$\tau_{|\Omega^\ell\setminus\Omega^{\ell+1}} = \psi_{|\Omega^\ell\setminus\Omega^{\ell+1}}, \tag{5}$$

that is used in the proof of the following theorem.

Theorem 2.2. *By assuming that property (P1) hold for the basis Ψ^ℓ, for $\ell = 0,\ldots,N-1$, the truncated hierarchical spline basis $\mathcal{T}$ is linearly independent.*

Proof. Since a truncated function of level ℓ coincides with its mother function in $\Omega^\ell \setminus \Omega^{\ell+1}$, the proof is completely analogous to the one of [26, Proposition 9], simply replacing the use of local linear independence by property (P1) as it was done in the proof of Theorem 2.1. □

In addition to the linear independence of the hierarchical basis $\mathcal{H}$ and the truncated hierarchical basis $\mathcal{T}$, the following properties also hold as in the C^1 construction for two-patch domains [11, Proposition 1] and the abstract setting in [26, Proposition 9] for the truncated basis, see those references for details. First, the intermediate spline spaces are nested. Second, given a hierarchy of subdomains defined at each level as an enlargement of $(\Omega^\ell)_{\ell=0,\dots,N-1}$, the original hierarchical spline space is a subspace of the hierarchical spline space defined over the considered enlarged subdomains. And third, the hierarchical spline space generated by the truncated basis in (3) coincides with the span of the hierarchical basis introduced in (1). Furthermore, the non-negativity and the partition of unity properties also hold for the truncated basis, provided that they hold at every level and the coefficients in the two-scale relation are positive. We have removed these two properties from the abstract framework, because the C^1 basis functions that we will use in the following do not satisfy them.

3 C^1 splines on the multi-patch setting

In this section we describe the geometric configuration and the C^1 spline spaces for one single level, following the notation in [11, 37, 36] with small changes. We start with a description of the geometry, and then we introduce the C^1 spline space.

3.1 The geometric multi-patch setting

Let us consider an open domain $\Omega \subset \mathbb{R}^2$, which is built up of quadrilateral patches $\Omega^{(i)}$, $i \in \mathcal{I}_\Omega$, with $\Omega^{(i)} \cap \Omega^{(j)} = \emptyset$ for $i \neq j$, inner edges $\Sigma^{(i)}$, $i \in \mathcal{I}_\Sigma^\circ$, and inner vertices $\mathbf{x}^{(i)}$, $i \in \mathcal{I}_\chi^\circ$, i.e.

$$\Omega = \left(\bigcup_{i \in \mathcal{I}_\Omega} \Omega^{(i)} \right) \cup \left(\bigcup_{i \in \mathcal{I}_\Sigma^\circ} \Sigma^{(i)} \right) \cup \left(\bigcup_{i \in \mathcal{I}_\chi^\circ} \mathbf{x}^{(i)} \right),$$

and whose boundary $\Gamma = \partial\Omega$ is the union of boundary edges $\Sigma^{(i)}$, $i \in \mathcal{I}_\Sigma^\Gamma$, and boundary vertices $\mathbf{x}^{(i)}$, $i \in \mathcal{I}_\chi^\Gamma$, i.e.

$$\Gamma = \left(\bigcup_{i \in \mathcal{I}_\Sigma^\Gamma} \Sigma^{(i)} \right) \cup \left(\bigcup_{i \in \mathcal{I}_\chi^\Gamma} \mathbf{x}^{(i)} \right).$$

We assume that no hanging nodes exist, and denote by $\mathcal{I}_\Sigma$ and $\mathcal{I}_\chi$ the disjoint unions of indices for inner and boundary edges and vertices, respectively, that is, $\mathcal{I}_\Sigma = \mathcal{I}_\Sigma^\circ \dot\cup \mathcal{I}_\Sigma^\Gamma$ and $\mathcal{I}_\chi = \mathcal{I}_\chi^\circ \dot\cup \mathcal{I}_\chi^\Gamma$.

3.1.1 Univariate spaces and basis functions

Let $\mathbb{S}_p^r$ be the univariate spline space of degree $p \geq 3$ and regularity $1 \leq r \leq p-2$ in $[0,1]$ with respect to the uniform open knot vector

$$\Xi_p^r = (\ \underbrace{0,\dots,0}_{(p+1)-\text{times}}\ ,\underbrace{\tfrac{1}{k+1}\cdots,\tfrac{1}{k+1}}_{(p-r)-\text{times}},\underbrace{\tfrac{2}{k+1},\dots,\tfrac{2}{k+1}}_{(p-r)-\text{times}},\dots,\underbrace{\tfrac{k}{k+1},\dots,\tfrac{k}{k+1}}_{(p-r)-\text{times}},\ \underbrace{1,\dots,1}_{(p+1)-\text{times}}\ ),$$

with $k \in \mathbb{N}_0$ and $k \geq \max(0, \frac{5-p}{p-r-1})$, and let $N_{j,p}^r$, $j \in \{0,\dots,n-1\}$ with $n = p+1+k(p-r)$, be the associated B-splines. We will also need the subspaces $\mathbb{S}_p^{r+1}$ and $\mathbb{S}_{p-1}^r$ defined from the same internal breakpoints $\frac{j}{k+1}$, $j = 0,1,\dots,k$, and will use for their B-splines the analogous notation $N_{j,p}^{r+1}$, $j \in \{0,\dots,n_0-1\}$, and $N_{j,p-1}^r$, $j \in \{0,\dots,n_1-1\}$, respectively, where $n_0 = p+1+k(p-r-1)$ and $n_1 = p+k(p-r-1)$.

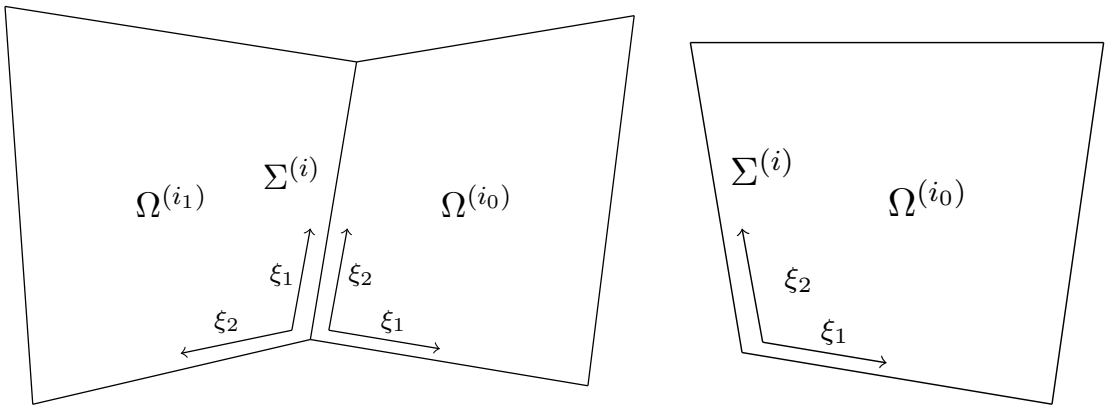

Figure 1: Representation in standard form with respect to an edge $\Sigma^{(i)}$, $i \in \mathcal{I}_\Sigma$. Left: Two neighboring patches $\Omega^{(i_0)}$ and $\Omega^{(i_1)}$ with common inner edge $\Sigma^{(i)}$, $i \in \mathcal{I}_\Sigma^\circ$. Right: The patch $\Omega^{(i_0)}$ with boundary edge $\Sigma^{(i)}$, $i \in \mathcal{I}_\Sigma^\Gamma$.

Moreover, we will use the modified basis functions $M_{j,p}^r$, for $j = 0, 1$, $M_{j,p}^{r+1}$, for $j = 0, 1, 2$, and $M_{j,p-1}^r$, for $j = 0, 1$, which fulfill

$$\begin{aligned}
&\partial_\xi^i M_{j,p}^r(0) = \delta_j^i, \text{ for } i, j = 0, 1,\\
&\partial_\xi^i M_{j,p}^{r+1}(0) = \delta_j^i, \text{ for } i, j = 0, 1, 2,\\
&\partial_\xi^i M_{j,p-1}^r(0) = \delta_j^i, \text{ for } i, j = 0, 1,
\end{aligned}$$

where δ_j^i is the Kronecker delta. Details of their definitions are given in Appendix A.1.

3.1.2 Parameterizations in standard configuration

Each quadrilateral patch $\Omega^{(i)}$, $i \in \mathcal{I}_\Omega$, is given as the open image of a bijective and regular geometry mapping

$$\mathbf{F}^{(i)} : [0, 1]^2 \to \overline{\Omega^{(i)}},$$

with $\mathbf{F}^{(i)} \in (\mathbb{S}_p^r \otimes \mathbb{S}_p^r)^2$. The resulting multi-patch parameterization (also called multi-patch geometry) of Ω, which consists of the single spline parameterizations $\mathbf{F}^{(i)}$, $i \in \mathcal{I}_\Omega$, will be denoted by $\mathbf{F}$.

Considering a particular edge $\Sigma^{(i)}$, $i \in \mathcal{I}_\Sigma$, or vertex $\mathbf{x}^{(i)}$, $i \in \mathcal{I}_\chi$, we will assume throughout the paper that the geometry mappings $\mathbf{F}^{(i_m)}$ of the corresponding patches $\Omega^{(i_m)}$ in the vicinity of the edge or vertex are given in standard form (see [37, 36]). In case of an edge $\Sigma^{(i)}$, $i \in \mathcal{I}_\Sigma$, we distinguish between an inner and a boundary edge. For any inner edge $\Sigma^{(i)}$, $i \in \mathcal{I}_\Sigma^\circ$, we assume that the two patches $\Omega^{(i_0)}$ and $\Omega^{(i_1)}$, $i_0, i_1 \in \mathcal{I}_\Omega$, with $\Sigma^{(i)} \subset \overline{\Omega^{(i_0)}} \cup \overline{\Omega^{(i_1)}}$, are parameterized in such a way that

$$\mathbf{F}^{(i_0)}(0, \xi) = \mathbf{F}^{(i_1)}(\xi, 0), \ \xi \in (0, 1),$$

see Fig. 1 (left). Similarly, for any boundary edge $\Sigma^{(i)}$, $i \in \mathcal{I}_\Sigma^\Gamma$, the geometry mapping $\mathbf{F}^{(i_0)}$ of the associated patch $\Omega^{(i_0)}$, $i_0 \in \mathcal{I}_\Omega$, with $\Sigma^{(i)} \subset \overline{\Omega^{(i_0)}}$, fulfills

$$\Sigma^{(i)} = \mathbf{F}^{(i_0)}(0, (0, 1)),$$

see Fig. 1 (right).

In case of a vertex $\mathbf{x}^{(i)}$, $i \in \mathcal{I}_\chi$, we distinguish between an inner and a boundary vertex. For any inner vertex $\mathbf{x}^{(i)}$, $i \in \mathcal{I}_\chi^\circ$, with patch valence $\nu_i \geq 3$, we respectively denote the patches and edges around the

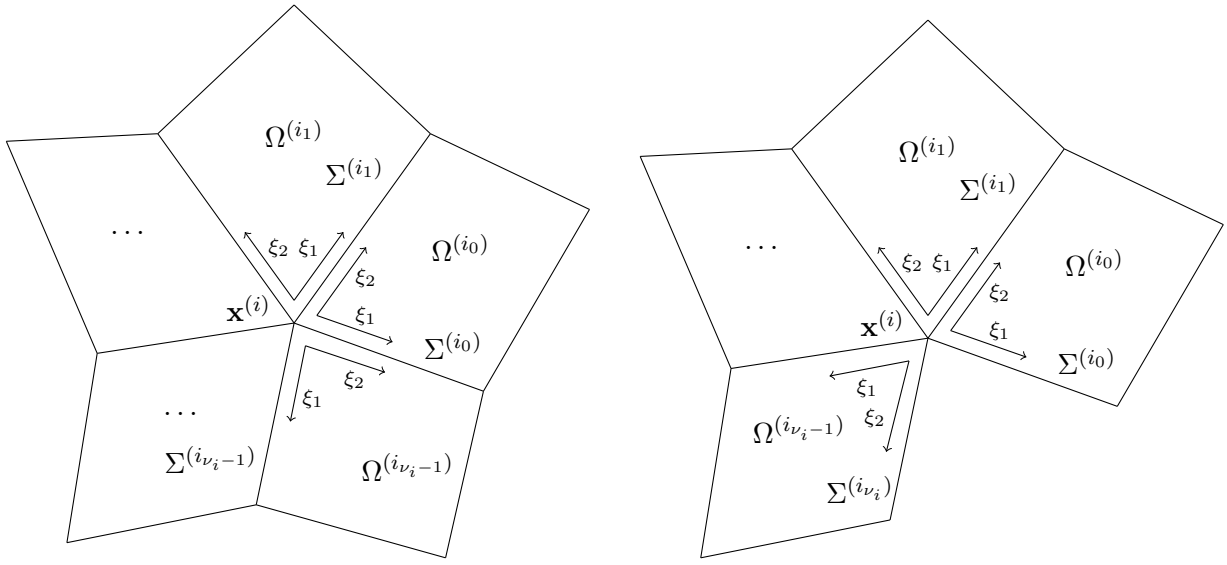

Figure 2: Representation in standard form with respect to a vertex $\mathbf{x}^{(i)}$, $i \in \mathcal{I}_\chi$. Left: Edges $\Sigma^{(i_0)}$, ..., $\Sigma^{(i_{\nu_i-1})}$ and patches $\Omega^{(i_0)}$, ..., $\Omega^{(i_{\nu_i-1})}$ around a common inner vertex $\mathbf{x}^{(i)}$, $i \in \mathcal{I}_\chi^\circ$. Right: Edges $\Sigma^{(i_0)}$, ..., $\Sigma^{(i_{\nu_i})}$ and patches $\Omega^{(i_0)}$, ..., $\Omega^{(i_{\nu_i-1})}$ around a common boundary vertex $\mathbf{x}^{(i)}$, $i \in \mathcal{I}_\chi^\Gamma$.

vertex $\mathbf{x}^{(i)}$ in counterclockwise order by $\Omega^{(i_m)}$ and $\Sigma^{(i_m)}$, for $m = 0, \ldots, \nu_i - 1$, see Fig. 2 (left). Moreover, we assume that the geometry mappings $\mathbf{F}^{(i_m)}$, $m = 0, \ldots, \nu_i - 1$, are parameterized in such a way that

$$\mathbf{x}^{(i)} = \mathbf{F}^{(i_m)}(0,0) \ \text{ for } m = 0, \ldots, \nu_i - 1,$$

and

$$\Sigma^{(i_{m+1})} = \mathbf{F}^{(i_m)}(0,(0,1)) = \mathbf{F}^{(i_{m+1})}((0,1),0) \ \text{ for } m = 0, \ldots, \nu_i - 1,$$

where the index m is considered to be modulo ν_i. Similarly, for any boundary vertex $\mathbf{x}^{(i)}$, $i \in \mathcal{I}_\chi^\Gamma$, with patch valence $\nu_i \geq 1$, the patches and edges around the vertex $\mathbf{x}^{(i)}$ are labeled in counterclockwise order by $\Omega^{(i_m)}$, for $m = 0, \ldots, \nu_i - 1$, and $\Sigma^{(i_m)}$, for $m = 0, \ldots, \nu_i$, see Fig. 2 (right). Further, the geometry mappings $\mathbf{F}^{(i_m)}$, $m = 0, \ldots, \nu_i - 1$, are parameterized in such a way that

$$\mathbf{x}^{(i)} = \mathbf{F}^{(i_m)}(0,0) \ \text{ for } m = 0, \ldots, \nu_i - 1,$$

the inner edges $\Sigma^{(i_{m+1})}$ are given as

$$\Sigma^{(i_{m+1})} = \mathbf{F}^{(i_m)}(0,(0,1)) = \mathbf{F}^{(i_{m+1})}((0,1),0) \ \text{ for } m = 1, \ldots, \nu_i - 1,$$

while the boundary edges $\Sigma^{(i_0)}$ and $\Sigma^{(i_{\nu_i})}$ are

$$\Sigma^{(i_0)} = \mathbf{F}^{(i_0)}((0,1),0) \text{ and } \Sigma^{(i_{\nu_i})} = \mathbf{F}^{(i_{\nu_i-1})}(0,(0,1)).$$

Remark 3.1. *Obviously, the standard configuration cannot be attained around every vertex without changing the parameterizations. In fact, for each vertex $\mathbf{x}^{(i)}$, $i \in \mathcal{I}_\chi$, with patch valence ν_i one would have to define a suitable parameterization $\mathbf{G}_\chi^{(i,m)}$ of $\Omega^{(i_m)}$, for $m = 0, \ldots, \nu_i - 1$, to recover the standard configuration. These parameterizations are obtained from $\mathbf{F}^{(i_m)}$ by possibly reversing each one of the parametric directions, and swapping them, which gives a total of eight possible combinations (four if the Jacobian is assumed to be positive). Similar parameterizations $\mathbf{G}_\Sigma^{(i,0)}$ and $\mathbf{G}_\Sigma^{(i,1)}$ would be also needed for the standard configuration on each edge. We have preferred to keep $\mathbf{F}^{(i_m)}$ to alleviate notation.*

3.1.3 Analysis-suitable G^1 parameterizations and gluing data

From now on we restrict ourselves to a particular class of multi-patch geometries $\mathbf{F}$, called analysis-suitable G^1 multi-patch parameterizations, which possess for each inner edge $\Sigma^{(i)}$, $i \in \mathcal{I}_\Sigma^\circ$, linear functions $\alpha^{(i,0)}$, $\alpha^{(i,1)}$, $\beta^{(i,0)}$ and $\beta^{(i,1)}$, with $\alpha^{(i,0)}$ and $\alpha^{(i,1)}$ relatively prime, such that for all $\xi \in [0,1]$

$$\alpha^{(i,0)}(\xi)\alpha^{(i,1)}(\xi) > 0$$

and

$$\alpha^{(i,0)}(\xi)\partial_2\mathbf{F}^{(i_1)}(\xi,0) + \alpha^{(i,1)}(\xi)\partial_1\mathbf{F}^{(i_0)}(0,\xi) + \beta^{(i)}(\xi)\partial_2\mathbf{F}^{(i_0)}(0,\xi) = \mathbf{0},$$

with

$$\beta^{(i)}(\xi) = \alpha^{(i,0)}(\xi)\beta^{(i,1)}(\xi) + \alpha^{(i,1)}(\xi)\beta^{(i,0)}(\xi), \tag{6}$$

see [20, 37]. This class of parameterization is exactly the one which allows the design of C^1 isogeometric spaces with optimal polynomial reproduction properties [20, 35]. Details for the computation of the gluing data are given in Appendix A.2. We note that, for each boundary edge $\Sigma^{(i)}$, $i \in \mathcal{I}_\Sigma^\Gamma$, we can simply assign trivial functions $\alpha^{(i,0)} \equiv 1$ and $\beta^{(i,0)} \equiv 0$.

Examples of analysis-suitable G^1 multi-patch geometries are e.g. piecewise bilinear parameterizations [20, 33, 39], but there exist different methods to generate from a given, possibly non-analysis-suitable G^1 multi-patch geometry, an analysis-suitable G^1 parameterization, see [35, 36].

In addition we define, for each inner edge $\Sigma^{(i)}$ with $i \in \mathcal{I}_\Sigma^\circ$, the vectors

$$\mathbf{t}^{(i)}(\xi) = \partial_2\mathbf{F}^{(i_0)}(0,\xi) = \partial_1\mathbf{F}^{(i_1)}(\xi,0),$$

and

$$\begin{aligned}\mathbf{d}^{(i)}(\xi) &= \tfrac{1}{\alpha^{(i,0)}(\xi)}\left(\partial_1\mathbf{F}^{(i_0)}(0,\xi) + \beta^{(i,0)}(\xi)\,\partial_2\mathbf{F}^{(i_0)}(0,\xi)\right)\\ &= -\tfrac{1}{\alpha^{(i,1)}(\xi)}\left(\partial_2\mathbf{F}^{(i_1)}(\xi,0) + \beta^{(i,1)}(\xi)\,\partial_1\mathbf{F}^{(i_1)}(\xi,0)\right).\end{aligned}$$

In case of a boundary edge $\Sigma^{(i)}$, $i \in \mathcal{I}_\Sigma^\Gamma$, with

$$\Sigma^{(i)} = \mathbf{F}^{(i_0)}(0,(0,1)),$$

we use the same definitions based only on the parameterization $\mathbf{F}^{(i_0)}$, noting that $\alpha^{(i,0)} \equiv 1$ and $\beta^{(i,0)} \equiv 0$.

3.2 The C^1 multi-patch isogeometric spline space

We now define the C^1 spline space on one level, and a particular subspace which maintains the same numerical approximation properties.

3.2.1 Construction of a particular C^1 isogeometric subspace

The C^1 isogeometric space $\mathbb{V}$ with respect to the multi-patch geometry $\mathbf{F}$ is given by

$$\mathbb{V} = \{\phi \in C^1(\overline{\Omega}) \ : \ \phi \circ \mathbf{F}^{(i)} \in \mathbb{S}_p^r \otimes \mathbb{S}_p^r, i \in \mathcal{I}_\Omega\}. \tag{7}$$

The space is associated to a mesh, determined by the knot vectors of the univariate spaces $\mathbb{S}_p^r$ and the parameterization $\mathbf{F}$, that we denote by G.

Since the space $\mathbb{V}$ has already for the case of two patches a complex structure and its dimension depends on the geometry [34], we consider instead the simpler subspace $\mathbb{A}$ firstly introduced in [37], which maintains the numerical approximation properties of $\mathbb{V}$ and whose dimension is independent of the geometry. The space $\mathbb{A}$ is defined as

$$\begin{aligned}&\mathbb{A} = \operatorname{span}\Phi, \qquad \Phi = \Phi_\Omega \cup \Phi_\Sigma \cup \Phi_\chi, \\ &\text{with } \Phi_\Omega = \bigcup_{i\in\mathcal{I}_\Omega} \Phi_{\Omega^{(i)}},\ \Phi_\Sigma = \bigcup_{i\in\mathcal{I}_\Sigma} \Phi_{\Sigma^{(i)}},\ \Phi_\chi = \bigcup_{i\in\mathcal{I}_\chi} \Phi_{\mathbf{x}^{(i)}},\end{aligned} \tag{8}$$

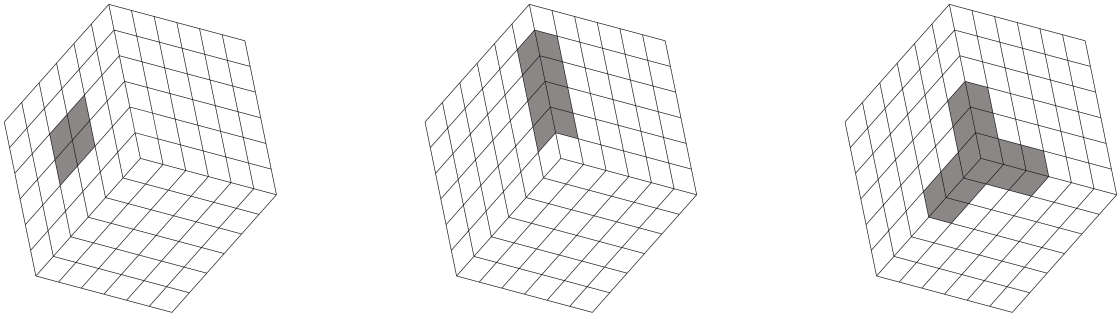

(a) Patch interior basis function. (b) Edge basis function. (c) Vertex basis function.

Figure 3: Example of maximal support of a patch interior basis function (left), an edge basis function (center) and a vertex basis function (right) for degree $p = 3$ and regularity $r = 1$.

where the three sets of basis functions are respectively called patch interior, edge and vertex basis functions, and are defined in detail below. All functions are generated in such a way that they are C^1-smooth on Ω and for the case of vertex functions even C^2-smooth at the corresponding vertex $\mathbf{x}^{(i)}$. To ensure the design of the space $\mathbb{A}$, a minimal number k of different inner knots is needed, given by $k \geq \max(0, \frac{5-p}{p-r-1})$, as already requested in the definition of the spline space $\mathbb{S}_p^r$ in Section 3. Below, we summarize the construction of the single functions and refer to [37, 36] for more details.

3.2.2 Patch interior basis functions

The patch interior basis functions are "standard" isogeometric functions whose value and first derivatives are zero on every edge and vertex. We start defining the index sets

$$\widetilde{\mathbf{J}}_\Omega = \{(j_1, j_2) : j_1, j_2 = 0, \dots, n-1\},$$
$$\mathbf{J}_\Omega = \{(j_1, j_2) : j_1, j_2 = 2, \dots, n-3\} \subset \widetilde{\mathbf{J}}_\Omega.$$

Then, for each patch $\Omega^{(i)}$, $i \in \mathcal{I}_\Omega$, we define the set of patch interior basis functions as

$$\Phi_{\Omega^{(i)}} = \left\{ \phi_{\mathbf{j}}^{\Omega^{(i)}} \ : \ \mathbf{j} \in \mathbf{J}_\Omega \right\},$$

where the functions $\phi_{\mathbf{j}}^{\Omega^{(i)}}$, $\mathbf{j} = (j_1, j_2)$, are given by

$$\phi_{\mathbf{j}}^{\Omega^{(i)}}(\mathbf{x}) = \begin{cases} \left(N_{j_1,p}^r N_{j_2,p}^r \circ \left(\mathbf{F}^{(i)}\right)^{-1} \right)(\mathbf{x}) & \text{if } \mathbf{x} \in \overline{\Omega^{(i)}}, \\ 0 & \text{otherwise.} \end{cases}$$

Therefore, the functions in $\Phi_{\Omega^{(i)}}$ trivially have support contained in $\Omega^{(i)}$, and their value and their gradient vanish on the boundary of $\Omega^{(i)}$. Moreover, their maximal support is attained for regularity $r = p - 2$, and consists of $\lfloor \frac{p+1}{2} \rfloor^2$ elements, see Figure 3(a).

Note that a function $\phi_{\mathbf{j}}^{\Omega^{(i)}}$ can be also defined for any index $\mathbf{j}$ of the extended index set $\widetilde{\mathbf{J}}_\Omega$, and for later use we also define the sets

$$\widetilde{\Phi}_\Omega = \bigcup_{i \in \mathcal{I}_\Omega} \widetilde{\Phi}_{\Omega^{(i)}}, \text{ with } \widetilde{\Phi}_{\Omega^{(i)}} = \left\{ \phi_{\mathbf{j}}^{\Omega^{(i)}} \ : \ \mathbf{j} \in \widetilde{\mathbf{J}}_\Omega \right\}.$$

However, the functions in $\widetilde{\Phi}_\Omega \setminus \Phi_\Omega$ do not belong to the space $\mathbb{A}$, and for this reason we call them "extended" patch interior functions.

3.2.3 Edge basis functions

Edge basis functions have support in the two patches adjacent to the edge, or one patch for boundary edges. We start defining the index sets

$$\widetilde{\mathbf{J}}_\Sigma = \{(j_1, j_2) : j_1 = 0, \dots, n_{j_2} - 1;\ j_2 = 0, 1\},$$
$$\mathbf{J}_\Sigma = \{(j_1, j_2) : j_1 = 3 - j_2, \dots, n_{j_2} - 4 + j_2;\ j_2 = 0, 1\} \subset \widetilde{\mathbf{J}}_\Sigma.$$

Then, for each edge $\Sigma^{(i)}$, $i \in \mathcal{I}_\Sigma$, and assuming the same orientation described in Section 3, we define the set of edge basis functions associated to the edge $\Sigma^{(i)}$ as

$$\Phi_{\Sigma^{(i)}} = \left\{ \phi_{\mathbf{j}}^{\Sigma^{(i)}} \ :\ \mathbf{j} \in \mathbf{J}_\Sigma \right\},$$

where each basis function $\phi_{\mathbf{j}}^{\Sigma^{(i)}}$, with $\mathbf{j} = (j_1, j_2)$, is defined as

$$\phi_{\mathbf{j}}^{\Sigma^{(i)}}(\mathbf{x}) = \begin{cases} \left(f_{(j_1,j_2)}^{(i,m)} \circ \left(\mathbf{F}^{(i_m)} \right)^{-1} \right)(\mathbf{x}) & \text{if } \mathbf{x} \in \overline{\Omega^{(i_m)}},\ m = 0, 1, \\ 0 & \text{otherwise,} \end{cases}$$

where the functions $f_{(j_1,j_2)}^{(i,m)}$ have been introduced in [37]. For convenience, we also give them in Appendix A.3.

It is easy to verify that the functions in $\Phi_{\Sigma^{(i)}}$ are supported in $\Omega^{(i_0)}$ and $\Omega^{(i_1)}$ (or $\Omega^{(i_0)}$ for boundary edges), and that their value, and first and second derivatives vanish on $\partial\Sigma^{(i)}$. Moreover, the maximal support of an edge function consists of $2(p+1)$ elements, with $p+1$ elements on each patch, see Figure 3(b).

Analogously to the patch interior functions, we can also define the edge function $\phi_{\mathbf{j}}^{\Sigma^{(i)}}$ for each index $\mathbf{j} \in \widetilde{\mathbf{J}}_\Sigma$, giving the sets of functions

$$\widetilde{\Phi}_\Sigma = \bigcup_{i \in \mathcal{I}_\Sigma} \widetilde{\Phi}_{\Sigma^{(i)}},\ \text{with } \widetilde{\Phi}_{\Sigma^{(i)}} = \left\{ \phi_{\mathbf{j}}^{\Sigma^{(i)}} \ :\ \mathbf{j} \in \widetilde{\mathbf{J}}_\Sigma \right\}.$$

However, the functions in $\widetilde{\Phi}_\Sigma \setminus \Phi_\Sigma$ do not belong to the space $\mathbb{A}$, so we call them "extended" edge functions.

Remark 3.2. *In the definition of $f_{(j_1,j_2)}^{(i,m)}$, the subindex j_2, refers to the type of edge basis functions: the values 0 and 1 respectively refer to* trace *and* derivative *edge functions. These were denoted by Φ^{Γ_0} and Φ^{Γ_1} in [11]. We have preferred to follow the indexing in [37, 36], to reduce the number of symbols.*

3.2.4 Vertex basis functions

Vertex basis functions have support in all the patches adjacent to the vertex. There are always six vertex functions associated to each vertex, independently of its valence. We start defining the index set

$$\mathbf{J}_\chi = \{(j_1, j_2) : j_1, j_2 = 0, 1, 2;\ j_1 + j_2 \leq 2\},$$

and then for each vertex $\mathbf{x}^{(i)}$, $i \in \mathcal{I}_\chi$ we define the set of vertex basis functions as

$$\Phi_{\mathbf{x}^{(i)}} = \left\{ \phi_{\mathbf{j}}^{\mathbf{x}^{(i)}} \ :\ \mathbf{j} \in \mathbf{J}_\chi \right\}.$$

To define the vertex basis functions $\phi_{\mathbf{j}}^{\mathbf{x}^{(i)}}$, and recalling that the patch valence is denoted by ν_i, we first define the factor

$$\sigma_i = \left(\frac{1}{p(k+1)\nu_i} \sum_{m=0}^{\nu_i - 1} \|\nabla \mathbf{F}^{(i_m)}(0,0)\|_\infty \right)^{-1}, \tag{9}$$

which will be used to uniformly scale the vertex functions with respect to the infinity norm. Then, for each index $\mathbf{j} = (j_1, j_2) \in \mathbf{J}_\chi$, the corresponding vertex function is defined as

$$\phi_{\mathbf{j}}^{\mathbf{x}^{(i)}}(\mathbf{x}) = \begin{cases} \sigma_i^{j_1+j_2} \left(\left(g_{\mathbf{j}}^{(i,m,\mathrm{prec})} + g_{\mathbf{j}}^{(i,m,\mathrm{next})} - h_{\mathbf{j}}^{(i,m)} \right) \circ \left(\mathbf{F}^{(i_m)} \right)^{-1} \right)(\mathbf{x}) \\ \qquad\qquad \text{if } \mathbf{x} \in \overline{\Omega^{(i_m)}},\ m = 0, \dots, \nu_i - 1, \\ 0 \qquad\qquad \text{otherwise,} \end{cases} \tag{10}$$

where the functions $g_{\mathbf{j}}^{(i,m,\mathrm{prec})}$ and $g_{\mathbf{j}}^{(i,m,\mathrm{next})}$ respectively involve the edge preceding and following the patch $\Omega^{(i_m)}$, in counterclockwise direction, while the function $h_{\mathbf{j}}^{(i,m)}$ uses information from both edges. These functions were defined in [37], and for convenience we show their expressions in Appendix A.3.

The construction of the vertex functions $\phi_{\mathbf{j}}^{\mathbf{x}^{(i)}}$, for $\mathbf{j} \in \mathbf{J}_\chi$, ensures that their support is contained in the patches around the vertex $\mathbf{x}^{(i)}$, and

$$\partial_1^{z_1} \partial_2^{z_2} \left(\phi_{\mathbf{j}}^{\mathbf{x}^{(i)}} \right)(\mathbf{x}^{(i)}) = \sigma_i^{j_1+j_2} \delta_{j_1}^{z_1} \delta_{j_2}^{z_2},\ 0 \le z_1, z_2 \le 2,\ z_1 + z_2 \le 2, \tag{11}$$

see [37]. Moreover, the support of a vertex basis function consists at most of five elements per patch, for a total of $5\nu_i$ elements, see Figure 3(c).

3.3 Representation of the basis in terms of standard B-splines

In the proofs of linear independence in Section 4.3, and also for an efficient implementation of the C^1 space, we will make use of the representation of the C^1 basis functions of the previous section in terms of the standard B-spline basis.

Let us use the notation

$$\boldsymbol{\phi}_{\Omega^{(i)}} = [\phi_{\mathbf{j}}^{\Omega^{(i)}}]_{\mathbf{j} \in \mathbf{J}_\Omega}, \quad \text{for } i \in \mathcal{I}_\Omega, \tag{12}$$

$$\boldsymbol{\phi}_{\Sigma^{(i)}} = [\phi_{\mathbf{j}}^{\Sigma^{(i)}}]_{\mathbf{j} \in \mathbf{J}_\Sigma}, \quad \text{for } i \in \mathcal{I}_\Sigma, \tag{13}$$

$$\boldsymbol{\phi}_{\mathbf{x}^{(i)}} = [\phi_{\mathbf{j}}^{\mathbf{x}^{(i)}}]_{\mathbf{j} \in \mathbf{J}_\chi}, \quad \text{for } i \in \mathcal{I}_\chi, \tag{14}$$

to respectively indicate the vectors of patch interior basis functions, of edge basis functions and of vertex basis functions. As we want to write them in terms of standard B-splines, we also introduce the vector of B-splines basis functions of the space $\mathbb{S}_p^r \otimes \mathbb{S}_p^r$ mapped into $\Omega^{(k)}$, given by

$$\mathbf{N}^{(k)} = [N_{j_1,p}^r N_{j_2,p}^r \circ (\mathbf{F}^{(k)})^{-1}]_{0 \le j_1, j_2 \le n-1}^T.$$

Moreover, introducing the set of indices $I = \{2, \dots, n-3\}$, we also define the subvectors

$$\begin{aligned} \mathbf{N}_0^{(k)} &= [N_{j_1,p}^r(\xi_1) N_{j_2,p}^r(\xi_2) \circ (\mathbf{F}^{(k)})^{-1}]_{j_1 \in \{0,1\}, j_2 \in \{0,1\}}, \\ \mathbf{N}_1^{(k)} &= [N_{j_1,p}^r(\xi_1) N_{j_2,p}^r(\xi_2) \circ (\mathbf{F}^{(k)})^{-1}]_{j_1 \in I, j_2 \in \{0,1\}}, \\ \mathbf{N}_2^{(k)} &= [N_{j_1,p}^r(\xi_1) N_{j_2,p}^r(\xi_2) \circ (\mathbf{F}^{(k)})^{-1}]_{j_1 \in \{0,1\}, j_2 \in I}, \\ \mathbf{N}_3^{(k)} &= [N_{j_1,p}^r(\xi_1) N_{j_2,p}^r(\xi_2) \circ (\mathbf{F}^{(k)})^{-1}]_{j_1 \in I, j_2 \in I}, \end{aligned} \tag{15}$$

respectively corresponding to the basis functions with nonzero value or nonzero first derivatives on the bottom left vertex, on the bottom edge (but zero on every vertex), on the left edge (but zero on every vertex), and internal functions with zero value and derivative on every edge. With some abuse of notation, we denote in the same way the vectors of B-spline functions extended by zero outside $\Omega^{(k)}$.

We first note that the patch interior basis functions in the vector $\boldsymbol{\phi}_{\Omega^{(i)}}$ have their support contained in the patch $\Omega^{(i)}$, where they coincide with standard B-splines, so their representation in terms of B-splines is trivially given by $\boldsymbol{\phi}_{\Omega^{(i)}} = \mathbf{N}_3^{(i)}$.

The edge basis functions associated with an edge $\Sigma^{(i)}$ in the multi-patch case are a subset of the edge functions for the two patch case. Recalling the notation for "extended" edge functions in the previous section, and introducing the corresponding vector of functions $\widetilde{\boldsymbol{\phi}}_{\Sigma^{(i)}} := [\phi_{\mathbf{j}}^{\Sigma^{(i)}}]_{\mathbf{j}\in\widetilde{\mathbf{J}}_\Sigma}$, we know from the two-patch case [34, 11] that edge functions can be written as standard B-splines in the form

$$\widetilde{\boldsymbol{\phi}}_{\Sigma^{(i)}} = \widetilde{E}_{i,0}\mathbf{N}^{(i_0)} + \widetilde{E}_{i,1}\mathbf{N}^{(i_1)}, \tag{16}$$

where the only B-splines that play a role are the ones with non-vanishing value or derivative on the edge. Therefore the relation for the multi-patch case is immediately given by

$$\boldsymbol{\phi}_{\Sigma^{(i)}} = E_{i,0}\mathbf{N}_2^{(i_0)} + E_{i,1}\mathbf{N}_1^{(i_1)}, \tag{17}$$

where $E_{i,k}$ is the submatrix of $\widetilde{E}_{i,k}$ containing only the rows corresponding to the edge functions in $\Phi_{\Sigma^{(i)}}$, i.e., to the indices $\mathbf{J}_\Sigma$, and the columns of B-splines with nonzero coefficients.

For the vertex basis functions associated with the vertex $\mathbf{x}^{(i)}$, from their definition (10) and equations (37)-(39) follows the relation

$$\boldsymbol{\phi}_{\mathbf{x}^{(i)}} = \sum_{m=0}^{\nu_i-1}\left(K_{i,m}\widehat{E}_{i_m,1}\begin{bmatrix}\mathbf{N}_0^{(i_m)}\\ \mathbf{N}_1^{(i_m)}\end{bmatrix} + K_{i,m+1}\widehat{E}_{i_{m+1},0}\begin{bmatrix}\mathbf{N}_0^{(i_m)}\\ \mathbf{N}_2^{(i_m)}\end{bmatrix} - V_{i,m}\mathbf{N}_0^{(i_m)}\right), \tag{18}$$

where $\Sigma^{(i_m)}$ and $\Sigma^{(i_{m+1})}$ are the two edges of the patch $\Omega^{(i_m)}$ containing the vertex $\mathbf{x}^{(i)}$, $\widehat{E}_{i_m,1}$ and $\widehat{E}_{i_{m+1},0}$ are the submatrices of $\widetilde{E}_{i_m,1}$ and $\widetilde{E}_{i_{m+1},0}$ containing only the rows corresponding to the five "extended" edge functions in $\widetilde{\Phi}_{\Sigma^{(i_m)}} \setminus \Phi_{\Sigma^{(i_m)}}$ and $\widetilde{\Phi}_{\Sigma^{(i_{m+1})}} \setminus \Phi_{\Sigma^{(i_{m+1})}}$ close to the vertex, respectively, and the columns with nonzero coefficients. The detailed computations which lead to the matrices $K_{i,m}$, $K_{i,m+1}$ and $V_{i,m}$, based on using the expression of the modified basis functions from Appendix A.1, are given in Appendix A.4 for general regularity $r \le p-2$. For convenience we give their expressions here for the case $r = p-2$.

The matrices $K_{i,m}$, $K_{i,m+1}$ are of size 6×5 and each one of their rows, which corresponds to a different value of $\mathbf{j} = (j_1, j_2)$, is of the form

$$\sigma_i^{j_1+j_2}\begin{bmatrix} c_{\mathbf{j},0}^{(i_s)} \\ c_{\mathbf{j},0}^{(i_s)} + \frac{c_{\mathbf{j},1}^{(i_s)}}{p(k+1)} \\ c_{\mathbf{j},0}^{(i_s)} + \frac{3c_{\mathbf{j},1}^{(i_s)}}{p(k+1)} + \frac{2c_{\mathbf{j},2}^{(i_s)}}{p(p-1)(k+1)^2} \\ \frac{d_{\mathbf{j},0}^{(i_s)}}{p(k+1)} \\ \frac{d_{\mathbf{j},0}^{(i_s)}}{p(k+1)} + \frac{d_{\mathbf{j},1}^{(i_s)}}{p(p-1)(k+1)^2} \end{bmatrix}^T, \quad s = m, m+1,$$

with σ_i being the factor in (9), and the $c_{\mathbf{j}}$ and $d_{\mathbf{j}}$ coefficients defined in Appendix A.3.

The matrix $V_{i,m}$ is of size 6×4 and each one of their rows, corresponding to a different value of $\mathbf{j} = (j_1, j_2)$, is then of the form

$$\sigma_i^{j_1+j_2}\begin{bmatrix} c_{\mathbf{j},0}^{(i_m)} \\ c_{\mathbf{j},0}^{(i_m)} + \frac{c_{\mathbf{j},1}^{(i_m)}}{p(k+1)} \\ c_{\mathbf{j},0}^{(i_m)} + \frac{c_{\mathbf{j},1}^{(i_{m+1})}}{p(k+1)} \\ c_{\mathbf{j},0}^{(i_m)} + \frac{\left(c_{\mathbf{j},1}^{(i_m)} + c_{\mathbf{j},1}^{(i_{m+1})} + \frac{e_{\mathbf{j},(1,1)}^{(i_m)}}{p(k+1)}\right)}{p(k+1)} \end{bmatrix}^T,$$

with the four columns corresponding to the four B-splines in $\mathbf{N}_0^{(i_m)}$, and we have used the relationships between the $e_{\mathbf{j}}$ and the $c_{\mathbf{j}}$ coefficients in Appendix A.3.

These considerations allow us to write all the C^1 basis functions restricted to the patch $\Omega^{(k)}$ as linear combinations of the (mapped) B-spline basis of $\mathbb{S}_p^r \otimes \mathbb{S}_p^r$. That is, there exists a matrix C_k such that $\boldsymbol{\phi}|_{\Omega^{(k)}} = C_k \mathbf{N}^{(k)}$, and using the notation in (12)–(14) the vector $\boldsymbol{\phi}|_{\Omega^{(k)}}$ collects all the non-vanishing basis functions on $\Omega^{(k)}$, i.e., the patch interior functions $\boldsymbol{\phi}_{\Omega^{(k)}}$, the edge functions $\boldsymbol{\phi}_{\Sigma^{(i)}}$ from the four edges on the boundary of $\Omega^{(k)}$, and the vertex functions $\boldsymbol{\phi}_{\mathbf{x}^{(i)}}$ from the four vertices on the boundary of $\Omega^{(k)}$. It is then possible, using standard techniques, to pass from the B-spline representation to the Bernstein polynomial representation, the so-called Bézier extraction.

Finally, since there is a one-to-one correspondence between "extended" patch interior functions and standard B-splines, and employing the latter representation, for a function $\phi \in \mathbb{A}$ we denote by $\mathbf{K}(\phi)$ the set of the triples $(i, j_1, j_2) \in \mathcal{I}_\Omega \times \widetilde{\mathbf{J}}_\Omega$ such that the corresponding coefficient $\widetilde{e}_{j_1,j_2}^{(i)}$ in the B-spline representation is nonzero, i.e.

$$\mathbf{K}(\phi) = \left\{ (i, j_1, j_2) \in \mathcal{I}_\Omega \times \widetilde{\mathbf{J}}_\Omega \,:\, \phi(\mathbf{x}) = \sum_{i \in \mathcal{I}_\Omega} \sum_{j_1=0}^{n-1} \sum_{j_2=0}^{n-1} \widetilde{e}_{j_1,j_2}^{(i)} \phi_{\mathbf{j}}^{\Omega^{(i)}}(\mathbf{x}),\ \widetilde{e}_{j_1,j_2}^{(i)} \neq 0 \right\}.$$

We use a similar notation for a set of functions $\Psi \subset \mathbb{A}$, namely

$$\mathbf{K}(\Psi) = \bigcup_{\psi \in \Psi} \mathbf{K}(\psi), \tag{19}$$

the interesting case being when $\Psi \subset \Phi$ is a subset of the basis.

4 Theoretical results for the C^1 spline space on one level

In the following we analyze some properties of the subspace $\mathbb{A}$ that will be needed to apply the construction of the hierarchical space. In particular, we focus on the characterization of the space, and new results about (local) linear independence of certain subsets of its basis.

4.1 Characterization of the space $\mathbb{V}$ and the subspace $\mathbb{A}$

The characterization of the subspace $\mathbb{A}$, that we will use to prove nestedness in the hierarchical construction, was only given implicitly in previous works. We introduce it here explicitly for the sake of clarity.

The space $\mathbb{V}$ in (7) can be characterized as follows (see [20, 37, 36]): A function ϕ belongs to the space $\mathbb{V}$ if and only if for each patch $\Omega^{(i)}$, $i \in \mathcal{I}_\Omega$, the functions $\phi \circ \mathbf{F}^{(i)}$ satisfy that

$$\phi \circ \mathbf{F}^{(i)} \in \mathbb{S}_p^r \otimes \mathbb{S}_p^r, \tag{20}$$

and for each inner edge $\Sigma^{(i)}$, $i \in \mathcal{I}_\Sigma^\circ$, with the two corresponding neighboring patches $\mathbf{F}^{(i_0)}$ and $\mathbf{F}^{(i_1)}$ possessing the same orientation as described in Section 3, the functions $\phi \circ \mathbf{F}^{(i_0)}$ and $\phi \circ \mathbf{F}^{(i_1)}$ fulfill

$$\left(\phi \circ \mathbf{F}^{(i_0)}\right)(0, \xi) = \left(\phi \circ \mathbf{F}^{(i_1)}\right)(\xi, 0),\ \xi \in [0, 1], \tag{21}$$

and

$$\alpha^{(i,0)}(\xi) \partial_2 \left(\phi \circ \mathbf{F}^{(i_1)}\right)(\xi, 0) + \alpha^{(i,1)}(\xi) \partial_1 \left(\phi \circ \mathbf{F}^{(i_0)}\right)(0, \xi) + \beta^{(i)}(\xi) \partial_2 \left(\phi \circ \mathbf{F}^{(i_0)}\right)(0, \xi) = 0$$

for $\xi \in [0, 1]$. Due to (6), the previous equation is further equivalent to

$$\begin{aligned} &\tfrac{1}{\alpha^{(i,0)}(\xi)} \left(\partial_1 \left(\phi \circ \mathbf{F}^{(i_0)}\right)(0, \xi) + \beta^{(i,0)}(\xi)\, \partial_2 \left(\phi \circ \mathbf{F}^{(i_0)}\right)(0, \xi)\right) = \\ &-\tfrac{1}{\alpha^{(i,1)}(\xi)} \left(\partial_2 \left(\phi \circ \mathbf{F}^{(i_1)}\right)(\xi, 0) + \beta^{(i,1)}(\xi)\, \partial_1 \left(\phi \circ \mathbf{F}^{(i_1)}\right)(\xi, 0)\right). \end{aligned} \tag{22}$$

We denote for each inner edge $\Sigma^{(i)}$, $i \in \mathcal{I}_\Sigma^\circ$, the equally valued terms (21) and (22) by the functions $f_0^{(i)} : [0, 1] \to \mathbb{R}$ and $f_1^{(i)} : [0, 1] \to \mathbb{R}$, respectively, which describe the trace and a specific directional derivative

of the function ϕ across the associated interface $\Sigma^{(i)}$, see e.g. [11, 20, 34] for more details. Analogously, we define for each boundary edge $\Sigma^{(i)}$, $i \in \mathcal{I}_\Sigma^\Gamma$, with the associated patch $\mathbf{F}^{(i_0)}$ possessing the same orientation as described in Section 3, the functions $f_0^{(i)}$ and $f_1^{(i)}$ as the left-hand sides of (21) and (22), respectively, where $f_1^{(i)}$ can be simplified due to the selection of $\alpha^{(i,0)} \equiv 1$ and $\beta^{(i,0)} \equiv 0$ for boundary edges.

Equations (20)–(22) fully characterize the space $\mathbb{V}$. Similarly, we can give a characterization for the subspace $\mathbb{A}$, that we state in the following proposition. The proof is a direct consequence of the construction of the basis functions, and is omitted.

Proposition 4.1. *A function ϕ belongs to $\mathbb{A}$ if and only if it satisfies the conditions* (20), (21) *and* (22), *and moreover for each edge $\Sigma^{(i)}$, $i \in \mathcal{I}_\Sigma$, the functions $f_0^{(i)}$ and $f_1^{(i)}$ fulfill*

$$f_0^{(i)} \in \mathbb{S}_p^{r+1} \text{ and } f_1^{(i)} \in \mathbb{S}_{p-1}^{r}, \tag{23}$$

respectively, and for each vertex $\mathbf{x}^{(i)}$, $i \in \mathcal{I}_\chi$, we have $\phi \in C^2(\mathbf{x}^{(i)})$.

4.2 Counterexample of local linear independence

We will briefly demonstrate on the basis of an example, that the C^1 basis functions Φ, and in particular the vertex functions $\Phi_{\mathbf{x}^{(i)}}$ for a vertex $\mathbf{x}^{(i)}$, $i \in \mathcal{I}_\chi$, can be locally linearly dependent. This means that there exists an element such that the restriction of non-vanishing functions to that element is linearly dependent.

We consider the three-patch domain Ω shown in Figure 4 (left), where the single patches $\Omega^{(i)}$, $i \in \{0, 1, 2\}$, are respectively the images of the bilinear geometry mappings

$$\mathbf{F}^{(0)}(\xi_1, \xi_2) = (2(\sqrt{3}+1)\xi_1 + (\sqrt{3}-3)\xi_2, -2(\sqrt{3}-1)\xi_1 + (3\sqrt{3}+1)\xi_2),$$

$$\mathbf{F}^{(1)}(\xi_1, \xi_2) = ((\sqrt{3}-3)\xi_1 - (3\sqrt{3}-1)\xi_2, (3\sqrt{3}+1)\xi_1 - (\sqrt{3}+3)\xi_2)$$

and

$$\mathbf{F}^{(2)}(\xi_1, \xi_2) = (-(3\sqrt{3}-1)\xi_1 + 2(\sqrt{3}+1)\xi_2, -(\sqrt{3}+3)\xi_1 - 2(\sqrt{3}-1)\xi_2),$$

and the three-patch geometry is analysis-suitable G^1 because each single patch is bilinear. Moreover, the three patches are given in the standard form of Section 3.1.2 with respect to the inner vertex, that we denote by $\mathbf{x}^{(0)}$, and is thus given by $\mathbf{x}^{(0)} = \mathbf{F}^{(i)}(0, 0)$ for $i = 0, 1, 2$.

We compute the basis of functions of the C^1 isogeometric spline space $\mathbb{A}$ for the case of C^1 bicubic splines, i.e., $p = 3$, $r = 1$ with $k = 5$, and consider the element $Q \in G$ given by $Q = \mathbf{F}^{(0)}((0, \frac{1}{6}) \times (\frac{1}{6}, \frac{1}{3}))$ and highlighted in Figure 4 (right). Restricting the basis functions to Q, we can verify that 18 basis functions are non-vanishing on this element. This directly implies that the basis functions of the space $\mathbb{A}$ are locally linearly dependent, because the maximum number of linearly independent spline basis functions on one element is $(p+1)^2$, which means for $p = 3$ at most 16 functions.

In fact, the local linear dependence on this element is caused by the vertex basis functions. To study this in more detail, let us consider the set $\Phi_{\mathbf{x}^{(0)}} = \left\{\phi_{\mathbf{j}}^{\mathbf{x}^{(0)}} : \mathbf{j} \in \mathbf{J}_\chi\right\}$, and restrict the six vertex functions of this set to the element $Q \in G$. It is easy to verify that each of the six functions is non-vanishing on Q, and simplifies there to $\phi_{\mathbf{j}}^{\mathbf{x}^{(0)}} = \sigma_0^{j_1+j_2}\left(g_{\mathbf{j}}^{(0,0,\text{next})} \circ \left(\mathbf{F}^{(0)}\right)^{-1}\right)$. Since all the six functions $g_{\mathbf{j}}^{(0,0,\text{next})}$, $\mathbf{j} \in \mathbf{J}_\chi$, are just linear combinations of the five same functions, see (37), the corresponding six functions $\phi_{\mathbf{j}}^{\mathbf{x}^{(0)}}$ are linearly dependent on Q. Thereby, it is interesting to note that the six functions $g_{\mathbf{j}}^{(0,0,\text{next})}$, $\mathbf{j} \in \mathbf{J}_\chi$, can be even represented on Q just as linear combinations of three common functions, namely of the edge functions

$$f_{(1,0)}^{(i_1,0)} \circ \left(\mathbf{F}^{(0)}\right)^{-1},\ f_{(2,0)}^{(i_1,0)} \circ \left(\mathbf{F}^{(0)}\right)^{-1} \text{ and } f_{(1,1)}^{(i_1,0)} \circ \left(\mathbf{F}^{(0)}\right)^{-1}.$$

Remark 4.2. *It is possible to ensure local linear independence of the C^1 spline spaces by assuming that the internal degree and regularity satisfy $r < p - 3$. For instance, quintic functions with C^1 regularity ($p = 5$, $r = 1$) are locally linearly independent. However, the interesting case of the highest allowed regularity, $r = p - 2$, is in general locally linearly dependent.*

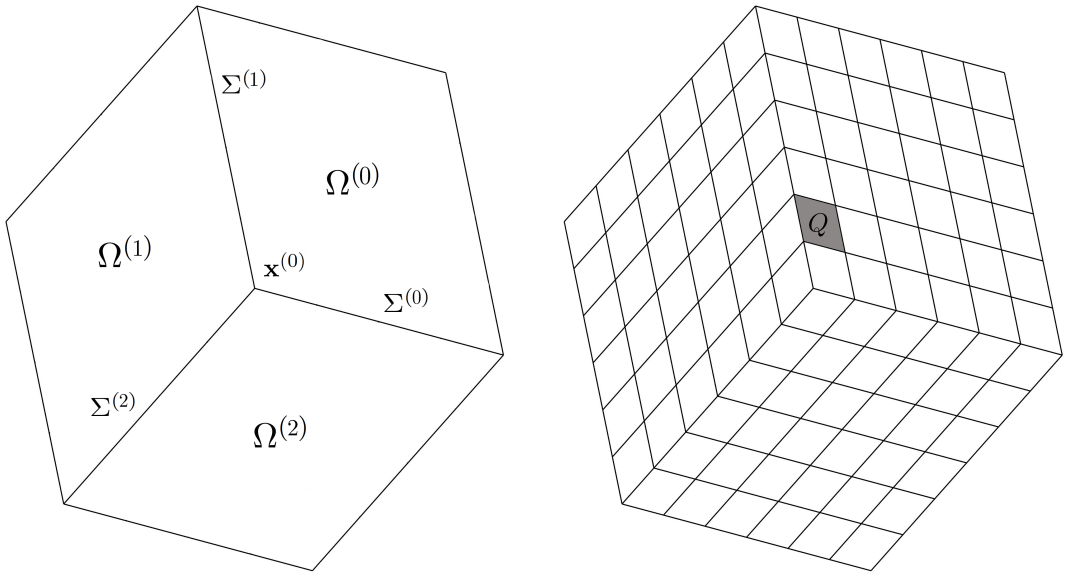

Figure 4: Left: A bilinearly parameterized three-patch domain Ω whose geometry mappings $\mathbf{F}^{(i)}$, $i \in \{0, 1, 2\}$, are given in standard configuration with respect to the inner vertex $\mathbf{x}^{(0)}$. Right: The associated set G of elements for $k = 5$ with a particular element $Q \in G$ given by $Q = \mathbf{F}^{(0)}((0, \frac{1}{6}) \times (\frac{1}{6}, \frac{1}{3}))$ and highlighted in gray.

4.3 Linear independence results for subsets of the basis

We will now study the (local) linear independence of particular subsets of the basis (8) of the C^1 isogeometric spline space $\mathbb{A}$. We first introduce and recall some needed notations and definitions.

Let Ψ be a set of functions in Ω. We say that Ψ is linearly independent in $\widetilde{\Omega} \subseteq \Omega$ if the set of functions

$$\Psi|_{\widetilde{\Omega}} := \{\beta|_{\widetilde{\Omega}} \,:\, \beta \in \Psi,\, \beta|_{\widetilde{\Omega}} \neq 0\}$$

is linearly independent. We further say that Ψ is locally linearly independent if $\Psi|_{\widetilde{\Omega}}$ is linearly independent for any $\widetilde{\Omega} \subseteq \Omega$.

Remark 4.3. *Since the basis functions are (mapped) piecewise polynomials on the mesh G, to show the local linear independence relations below it is sufficient to prove them just for any element $Q \in G$, instead of for any open domain $\widetilde{\Omega} \subseteq \Omega$.*

We can now state and prove some lemmas regarding the local linear independence properties. We start with some results for patch interior and edge basis functions, for which we will use the definition of the set in (19).

Lemma 4.4. *The "extended" set of patch (interior) functions $\widetilde{\Phi}_\Omega \supseteq \Phi_\Omega$ is locally linearly independent.*

Proof. The result follows from the local linear independence of tensor-product B-splines, noting that the supports of functions from two different patches only intersect on a vertex or an edge. □

Lemma 4.5. *Let $\overline{\Phi}, \widehat{\Phi} \subseteq \Phi$. If both $\overline{\Phi}$ and $\widehat{\Phi}$ are locally linearly independent, and if we further have*

$$\mathbf{K}(\overline{\Phi}) \cap \mathbf{K}(\widehat{\Phi}) = \emptyset, \tag{24}$$

then the union of functions $\overline{\Phi} \cup \widehat{\Phi}$ is locally linearly independent.

Proof. We prove the result by contradiction. Let us assume that the union of functions $\overline{\Phi} \cup \widehat{\Phi}$ is locally linearly dependent, which implies that there exists an element $Q \in G$ and nonzero coefficient vectors $\overline{\mathbf{d}} = \{\overline{d}_{\overline{\beta}}\}_{\overline{\beta} \in \overline{\Phi}} \neq \mathbf{0}$ and $\widehat{\mathbf{d}} = \{\widehat{d}_{\widehat{\beta}}\}_{\widehat{\beta} \in \widehat{\Phi}} \neq \mathbf{0}$ such that

$$\sum_{\overline{\beta} \in \overline{\Phi}} \overline{d}_{\overline{\beta}} \overline{\beta}|_Q + \sum_{\widehat{\beta} \in \widehat{\Phi}} \widehat{d}_{\widehat{\beta}} \widehat{\beta}|_Q = 0. \tag{25}$$

Note that both of the coefficient vectors $\overline{\mathbf{d}}$ and $\widehat{\mathbf{d}}$ have to be nonzero, since both set of functions $\overline{\Phi}$ and $\widehat{\Phi}$ are locally linearly independent. Equation (25) is further equivalent to

$$\sum_{\overline{\beta} \in \overline{\Phi}} \overline{d}_{\overline{\beta}} \overline{\beta}|_Q = -\sum_{\widehat{\beta} \in \widehat{\Phi}} \widehat{d}_{\widehat{\beta}} \widehat{\beta}|_Q. \tag{26}$$

Condition $\mathbf{K}(\overline{\Phi}) \cap \mathbf{K}(\widehat{\Phi}) = \emptyset$ implies that none of the "extended" patch interior functions which is part of the linear combination for the left term is also part of the linear combination for the right term and vice versa. This further implies, as a direct consequence of the local linear independence of the "extended" patch interior functions (see Lemma 4.4), that equation (26) is just possible if $\overline{\mathbf{d}} = \mathbf{0}$ and $\widehat{\mathbf{d}} = \mathbf{0}$, but this is clearly a contradiction to $\overline{\mathbf{d}} \neq \mathbf{0}$ and $\widehat{\mathbf{d}} \neq \mathbf{0}$. □

Lemma 4.6. *The set of patch interior and edge basis functions $\Phi_\Omega \cup \Phi_\Sigma$ is locally linearly independent.*

Proof. The local linear independence of the set of patch interior basis functions Φ_Ω directly follows from Lemma 4.4. For the set of edge basis functions Φ_Σ, for each edge the set $\Phi_{\Sigma^{(i)}}$, $i \in \mathcal{I}_\Sigma$, is locally linearly independent due to [11, Proposition 3], where the result was proved for the extended set $\widetilde{\Phi}_{\Sigma^{(i)}}$. By construction of the edge basis functions, and in particular due to (17), we have that

$$\mathbf{K}(\Phi_{\Sigma^{(i_1)}}) \cap \mathbf{K}(\Phi_{\Sigma^{(i_2)}}) = \emptyset$$

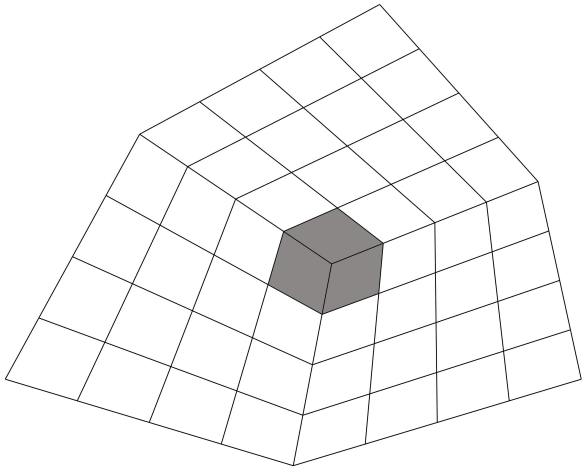

Figure 5: Example of the set of elements $G_{\mathbf{x}^{(i)}}$, highlighted in gray, adjacent to a vertex.

for any $i_1, i_2 \in \mathcal{I}_\Omega$, with $i_1 \neq i_2$, which further implies together with Lemma 4.5 that the set of edge basis functions $\Phi_\Sigma = \bigcup_{i \in \mathcal{I}_\Sigma} \Phi_{\Sigma^{(i)}}$ is locally linearly independent.

It remains to show that the union of patch interior and edge basis functions $\Phi_\Omega \cup \Phi_\Sigma$ is locally linearly independent. This is again a direct consequence of Lemma 4.5 using on the one hand the fact that each of the two sets is locally linearly independent, and on the other hand that, by construction of the individual basis functions, the two sets satisfy the condition

$$\mathbf{K}(\Phi_\Omega) \cap \mathbf{K}(\Phi_\Sigma) = \emptyset,$$

as can be clearly seen again from (17). □

For vertex basis functions local linear independence is not true in general, as we have seen in the counterexample of Section 4.2, but we can prove a partial result. To do so, we define for a vertex $\mathbf{x}^{(i)}$, $i \in \mathcal{I}_\chi$, the set of elements $Q \in G$ adjacent to the vertex $\mathbf{x}^{(i)}$, see Figure 5, and denote it by

$$G_{\mathbf{x}^{(i)}} := \{Q \in G : \mathbf{x}^{(i)} \in \partial Q\}.$$

Lemma 4.7. *For any $i \in \mathcal{I}_\chi$ and for every element $Q \in G_{\mathbf{x}^{(i)}}$, the vertex functions $\Phi_{\mathbf{x}^{(i)}}$ are linearly independent in Q.*

Proof. Let $\mathbf{x}^{(i)}$, $i \in \mathcal{I}_\chi$, be an arbitrary vertex, and let $Q \in G_{\mathbf{x}^{(i)}}$ be an arbitrary element adjacent to the vertex $\mathbf{x}^{(i)}$. By definition, the six vertex basis functions $\phi_{\mathbf{j}}^{\mathbf{x}^{(i)}}$, $\mathbf{j} \in \mathbf{J}_\chi$, do not vanish on Q, and they are uniquely determined by the C^2 interpolation condition (11) at the vertex $\mathbf{x}^{(i)}$, which yields their linear independence in Q. □

Finally, the next two lemmas show the relation between the different types of functions in the basis.

Lemma 4.8. *For any $m \in \mathcal{I}_\chi$, let us define*

$$\Psi_{\mathbf{x}^{(m)}} = \Phi \setminus \Phi_{\mathbf{x}^{(m)}} = \Phi_\Omega \cup \Phi_\Sigma \cup (\Phi_\chi \setminus \Phi_{\mathbf{x}^{(m)}}).$$

Then, for the set of vertex functions $\Phi_{\mathbf{x}^{(m)}}$ and for every element $Q \in G_{\mathbf{x}^{(m)}}$, it holds that $\operatorname{span}(\Phi_{\mathbf{x}^{(m)}}|_Q) \cap \operatorname{span}(\Psi_{\mathbf{x}^{(m)}}|_Q) = 0$.

Proof. Let the vertex $\mathbf{x}^{(m)}$, $m \in \mathcal{I}_\chi$, and the element $Q \in G_{\mathbf{x}^{(m)}}$. Due to Lemma 4.7, the six vertex basis functions in $\Phi_{\mathbf{x}^{(m)}}$ are linearly independent in Q, which was a direct result of their C^2 interpolation condition (11) at the vertex $\mathbf{x}^{(m)}$. Instead all other functions $\phi \in \Psi_{\mathbf{x}^{(m)}}$ satisfy by construction

$$\partial_1^{z_1}\partial_2^{z_2}\phi(\mathbf{x}^{(m)}) = 0,\ 0 \le z_1, z_2 \le 2,\ z_1 + z_2 \le 2,$$

which directly implies that the intersection of the spaces spanned by the two sets, restricted to Q, only contains the zero function. □

Lemma 4.9. *The space spanned by patch interior and edge basis functions and the space spanned by vertex basis functions, restricted to any element $Q \in G$, have trivial intersection, that is*

$$\operatorname{span}\left(\Phi_\Omega|_Q \cup \Phi_\Sigma|_Q\right) \cap \operatorname{span}\left(\Phi_\chi|_Q\right) = 0.$$

Proof. We have to prove for any $Q \in G$ that having

$$\sum_{i\in\mathcal{I}_\Omega,\mathbf{j}\in\mathbf{J}_\Omega} a_{i,\mathbf{j}}\phi_{\mathbf{j}}^{\Omega^{(i)}}|_Q + \sum_{i\in\mathcal{I}_\Sigma,\mathbf{j}\in\mathbf{J}_\Sigma} b_{i,\mathbf{j}}\phi_{\mathbf{j}}^{\Sigma^{(i)}}|_Q = \sum_{i\in\mathcal{I}_\chi,\mathbf{j}\in\mathbf{J}_\chi} c_{i,\mathbf{j}}\phi_{\mathbf{j}}^{\mathbf{x}^{(i)}}|_Q, \tag{27}$$

implies that both the left-hand side and the right-hand side are zero, for which it is sufficient to prove that one of them is zero.

We first recall that, by construction, any vertex basis function $\phi_{\mathbf{j}}^{\mathbf{x}^{(i)}}$ can be written as a linear combination of "extended" edge functions in $\bigcup_{m\in\mathcal{I}_\Sigma:\mathbf{x}^{(i)}\in\partial\Sigma^{(m)}}(\widetilde{\Phi}_{\Sigma^{(m)}} \setminus \Phi_{\Sigma^{(m)}})$ (the first and second terms in (18)), and the "extended" patch interior functions in $\bigcup_{m\in\mathcal{I}_\Omega:\mathbf{x}^{(i)}\in\partial\Omega^{(m)}}(\widetilde{\Phi}_{\Omega^{(m)}} \setminus \Phi_{\Omega^{(m)}})$ (the third term in (18)). In particular, the only "extended" patch interior functions in the linear combination that do not vanish have support in just one element, the element in the patch $\Omega^{(m)}$ adjacent to the vertex $\mathbf{x}^{(i)}$.

To prove the result we proceed by considering the restriction to the different types of elements: elements internal to a patch, elements adjacent to an edge but not to a vertex, and elements adjacent to a vertex.

If the element Q is internal to a patch, $\partial Q \cap \Sigma^{(i)} = \emptyset$ for every $i \in \mathcal{I}_\Sigma$, the right-hand side of (27) is zero by the support of vertex functions, and the result follows.

If the element Q is adjacent to an edge but not to a vertex, then $\partial Q \cap \Sigma^{(j)} \neq \emptyset$ for some $j \in \mathcal{I}_\Sigma$, and $\partial Q \cap \mathbf{x}^{(i)} = \emptyset$ for every $i \in \mathcal{I}_\chi$. Using the expression of vertex basis functions in terms of "extended" patch interior and edge functions, and the fact that "extended" patch interior functions have support in the element adjacent to the vertex, and therefore vanish in Q, we can replace the right-hand side in (27) by a sum on functions in $\widetilde{\Phi}_{\Sigma^{(j)}} \setminus \Phi_{\Sigma^{(j)}}$, i.e., the "extended" edge functions associated to edge $\Sigma^{(j)}$. Due to the result in [11, Proposition 3], which states the local linear independence of $\widetilde{\Phi}_{\Sigma^{(j)}} \cup (\Phi_{\Omega^{(j_0)}} \cup \Phi_{\Omega^{(j_1)}})$, all coefficients $a_{i,\mathbf{j}}$ and $b_{i,\mathbf{j}}$ are zero, and the result follows.

Finally, if the element Q is adjacent to a vertex, $\partial Q \cap \mathbf{x}^{(i)} \neq \emptyset$ (or equivalently, $Q \in G_{\mathbf{x}^{(i)}}$) for some $i \in \mathcal{I}_\chi$, by Lemma 4.8 the coefficients $c_{i,\mathbf{j}}$ in (27) associated to vertex functions in $\Phi_{\mathbf{x}^{(i)}}$ are zero. If the element is adjacent to more than one vertex, we can apply the same lemma subsequently to each vertex, and the result immediately follows. □

5 C^1 multi-patch hierarchical spline space

We now introduce the construction of the hierarchical C^1 spline space. We start by introducing the C^1 multi-patch spaces for each level, and then we analyze their properties to apply the construction of Section 2. In particular, we have to check the nestedness of the spaces, and that the assumptions of Theorem 2.1 are satisfied. As we will see, this will impose some constraints to modify the refinement algorithm.

5.1 C^1 multi-patch spaces on each level and hierarchical construction

Let us assume that we have a multi-patch domain Ω with an analysis-suitable G^1 parameterization $\mathbf{F}$ as in Section 3.1, and the C^1 space $\mathbb{V}^0$, with the corresponding subspace $\mathbb{A}^0$ as in Section 3.2. By successively

applying dyadic refinement, we construct a sequence of spaces $\mathbb{V}^\ell$ and their corresponding subspaces $\mathbb{A}^\ell$, for $\ell = 0, \dots, N-1$. The associated meshes are denoted by G^ℓ. To apply the construction of hierarchical splines from Section 2, the subspaces $\mathbb{A}^\ell$ and their bases Φ^ℓ respectively play the role of $\mathbb{U}^\ell$ and Ψ^ℓ in the construction of that section. We further assume that each subdomain Ω^ℓ is the union of elements of the mesh $G^{\ell-1}$. We will denote by $\mathcal{Q}$ the hierarchical mesh, and by $\mathcal{H}_{\mathbb{A}}$ the set of hierarchical C^1 splines, that we will prove to be a basis.

Note that the parameterizations, the geometric entities and the gluing data in Section 3.1 are independent of the level ℓ. Instead, the discrete spaces and their corresponding bases and basis functions clearly depend on ℓ, and we will use the ℓ superindex to refer to them. For instance, the basis will be denoted by Φ^ℓ, and the univariate spline spaces will be denoted by $\mathbb{S}_p^{r,\ell}$. Moreover, the set of elements from each level adjacent to a vertex will be denoted by $G^\ell_{\mathbf{x}^{(i)}}$.

In the following, we analyze the properties of the subspaces $\mathbb{A}^\ell$ to apply the construction of the hierarchical space.

5.2 Nestedness and refinement mask

The first property we need to prove is the nestedness of the subspaces, that is, that $\mathbb{A}^\ell \subset \mathbb{A}^{\ell+1}$ for $\ell = 0, \dots, N-2$. Nestedness is clear for the spaces $\mathbb{V}^\ell$, while for the subspaces $\mathbb{A}^\ell$ it relies on the characterization from Proposition 4.1.

Proposition 5.1. *Let $N \in \mathbb{N}$. The sequence of spaces $\mathbb{A}^\ell, \ell = 0, 1, \dots, N-1$ is nested, i.e.*

$$\mathbb{A}^0 \subset \mathbb{A}^1 \subset \ldots \subset \mathbb{A}^{N-1}.$$

Proof. The result is an immediate consequence of Proposition 4.1 and the nestedness of the univariate spline spaces, $\mathbb{S}_{p-1}^{r,\ell} \subset \mathbb{S}_{p-1}^{r,\ell+1}$ and $\mathbb{S}_p^{r+1,\ell} \subset \mathbb{S}_p^{r+1,\ell+1}$, for $\ell = 0, \dots, N-2$. □

Thanks to the nestedness of the subspaces $\mathbb{A}^\ell$, we can define the truncated hierarchical basis as described in Section 2, and we will denote it by $\mathcal{T}_{\mathbb{A}}$. The explicit definition of the functions in the truncated basis $\mathcal{T}_{\mathbb{A}}$ requires to use the coefficients of the two level relations between the C^1 basis functions of consecutive levels, also called the refinement mask, that we describe in the following.

Let us denote with an upper index ℓ the vectors of standard isogeometric functions (15) of level ℓ. Then, we have the relation between functions of two consecutive levels

$$\begin{bmatrix} \mathbf{N}_0^{(k),\ell} \\ \mathbf{N}_1^{(k),\ell} \\ \mathbf{N}_2^{(k),\ell} \\ \mathbf{N}_3^{(k),\ell} \end{bmatrix} = \begin{bmatrix} \Theta_{00}^{\ell+1} & \Theta_{01}^{\ell+1} & \Theta_{02}^{\ell+1} & \Theta_{03}^{\ell+1} \\ 0 & \Theta_{11}^{\ell+1} & 0 & \Theta_{13}^{\ell+1} \\ 0 & 0 & \Theta_{22}^{\ell+1} & \Theta_{23}^{\ell+1} \\ 0 & 0 & 0 & \Theta_{33}^{\ell+1} \end{bmatrix} \begin{bmatrix} \mathbf{N}_0^{(k),\ell+1} \\ \mathbf{N}_1^{(k),\ell+1} \\ \mathbf{N}_2^{(k),\ell+1} \\ \mathbf{N}_3^{(k),\ell+1} \end{bmatrix}, \text{ for } k \in \mathcal{I}_\Omega. \tag{28}$$

The refinement mask for the patch interior functions, which coincide with $\mathbf{N}_3^{(k),\ell}$, is simply a restriction of the relation (28) to their corresponding indices.

We recall that the edge functions, and "extended" edge functions, of level ℓ associated with an edge $\Sigma^{(i)}$, for $i \in \mathcal{I}_\Sigma$, can be expressed in terms of standard isogeometric functions through the matrix $\widetilde{E}_{i,k}^\ell$, as given by (16). Let us introduce the block diagonal matrix

$$\widetilde{\Lambda}^{\ell+1} = \begin{bmatrix} \widetilde{\Lambda}_p^{r+1,\ell+1} & 0 \\ 0 & \frac{1}{2}\widetilde{\Lambda}_{p-1}^{r,\ell+1} \end{bmatrix},$$

where $\widetilde{\Lambda}_q^{s,\ell+1}$ stands for the refinement matrix for univariate B-splines of level ℓ of degree q and regularity s. By generalizing the results in [11] for the two-patch case, and noting that functions in the subvectors $\mathbf{N}_3$ correspond to patch interior functions, we obtain the following refinement relation for the edge functions:

$$\boldsymbol{\phi}_{\Sigma^{(i)}}^\ell = \Lambda^{\ell+1}\boldsymbol{\phi}_{\Sigma^{(i)}}^{\ell+1} + E_{i,0}^\ell \Theta_{23}^{\ell+1} \mathbf{N}_3^{(i_0),\ell+1} + E_{i,1}^\ell \Theta_{13}^{\ell+1} \mathbf{N}_3^{(i_1),\ell+1} \tag{29}$$

$$= \Lambda^{\ell+1}\boldsymbol{\phi}_{\Sigma^{(i)}}^{\ell+1} + E_{i,0}^\ell \Theta_{23}^{\ell+1} \boldsymbol{\phi}_{\Omega^{(i_0)}}^{\ell+1} + E_{i,1}^\ell \Theta_{13}^{\ell+1} \boldsymbol{\phi}_{\Omega^{(i_1)}}^{\ell+1}, \tag{30}$$

where $\Lambda^{\ell+1}$ is the restriction of $\widetilde{\Lambda}^{\ell+1}$ to rows and columns corresponding to functions away from the vertices, and the matrices $E^{\ell}_{i,0}$ and $E^{\ell}_{i,1}$ are the matrices in (17) for basis functions of level ℓ.

For vertex basis functions, let us first introduce the diagonal matrix

$$D^{\ell+1}_{\mathbf{x}^{(i)}} = \operatorname{diag}\left(\left[1, \frac{\sigma^{\ell}_i}{\sigma^{\ell+1}_i}, \left(\frac{\sigma^{\ell}_i}{\sigma^{\ell+1}_i}\right)^2, \frac{\sigma^{\ell}_i}{\sigma^{\ell+1}_i}, \left(\frac{\sigma^{\ell}_i}{\sigma^{\ell+1}_i}\right)^2, \left(\frac{\sigma^{\ell}_i}{\sigma^{\ell+1}_i}\right)^2\right]\right).$$

Exploiting the expression for vertex functions in terms of standard isogeometric functions (18) and the refinement mask for extended edge functions from [11] and for standard mapped B-splines in (28), we obtain that for each vertex function of index $\mathbf{j} = (j_1, j_2) \in \mathbf{J}_\chi$ associated with the vertex $\mathbf{x}^{(i)}$, $i \in \mathcal{I}_\chi$, we have

$$\begin{aligned}\boldsymbol{\phi}^{\ell}_{\mathbf{x}^{(i)}} &= D^{\ell+1}_{\mathbf{x}^{(i)}} \boldsymbol{\phi}^{\ell+1}_{\mathbf{x}^{(i)}} + \sum_{m=0}^{\nu_i - 1} K^{\ell}_{i,m} \widehat{\Lambda}^{\ell+1} \boldsymbol{\phi}^{\ell+1}_{\Sigma^{(i_m)}} + \delta_b K^{\ell}_{i,\nu_i+1} \widehat{\Lambda}^{\ell+1} \boldsymbol{\phi}^{\ell+1}_{\Sigma^{(i_{\nu_i+1})}} \\ &+ \sum_{m=0}^{\nu_i - 1} \left(K^{\ell}_{i,m} \widehat{E}^{\ell}_{i_m,1} \begin{bmatrix} \Theta^{\ell+1}_{03} \\ \Theta^{\ell+1}_{13} \end{bmatrix} + K^{\ell}_{i,m+1} \widehat{E}^{\ell}_{i_{m+1},0} \begin{bmatrix} \Theta^{\ell+1}_{03} \\ \Theta^{\ell+1}_{23} \end{bmatrix} - V^{\ell}_{i,m} \Theta^{\ell+1}_{03} \right) \boldsymbol{\phi}^{\ell+1}_{\Omega^{(i_m)}},\end{aligned}$$

where δ_b indicates whether $\mathbf{x}^{(i)}$ is an interior or a boundary vertex, i.e.,

$$\delta_b = \begin{cases} 0 & \text{if } i \in \mathcal{I}^{\circ}_\chi, \\ 1 & \text{if } i \in \mathcal{I}^{\Gamma}_\chi, \end{cases}$$

$\widehat{\Lambda}^{\ell+1}$ is the restriction of $\widetilde{\Lambda}^{\ell+1}$ to rows corresponding to the five "extended" edge functions close to the vertex and to columns of active edge functions, while all the other matrices have been introduced above. Note that the Θ matrices appearing in the previous equation are very sparse, and in practice one can restrict the computations to the few coefficients that are nonzero.

5.3 Condition for linear independence of the hierarchical C^1 basis

The second property we need to prove is (P1), that guarantees linear independence of the hierarchical basis. The proof is based on the linear independence results from Section 4.3.

Theorem 5.2. *Let the spaces $\{\mathbb{A}^{\ell}\}_{\ell=0}^{N-1}$, with bases Φ^{ℓ}, obtained by dyadic refinement, the hierarchical mesh $\mathcal{Q}$, and let the hierarchical C^1 spline set $\mathcal{H}_{\mathbb{A}}$ be defined as in* (1)*, and $\mathcal{T}_{\mathbb{A}}$ be defined as in* (3)*. If for every active vertex function $\phi \in \Phi^{\ell}_{\mathbf{x}^{(i)}} \cap \mathcal{H}_{\mathbb{A}}$ there exists an active element $Q \in G^{\ell}_{\mathbf{x}^{(i)}} \cap \mathcal{Q}$, then both the functions in $\mathcal{H}_{\mathbb{A}}$ and the truncated functions in $\mathcal{T}_{\mathbb{A}}$ are linearly independent.*

Proof. We decompose the basis of each level $\Phi^{\ell} = \Phi^{\ell}_\Omega \cup \Phi^{\ell}_\Sigma \cup \Phi^{\ell}_\chi$ into $\#\mathcal{I}_\chi + 1$ sets as

$$\Phi^{\ell} = (\Phi^{\ell}_\Omega \cup \Phi^{\ell}_\Sigma) \cup \Big(\bigcup_{i \in \mathcal{I}_\chi} \Phi^{\ell}_{\mathbf{x}^{(i)}} \Big),$$

and therefore to apply Theorem 2.1 for $\mathcal{H}_{\mathbb{A}}$, or Theorem 2.2 for $\mathcal{T}_{\mathbb{A}}$, we have to prove property (P1) for each of the sets in the last term: patch interior and edge basis functions on the one hand, and each set of vertex basis functions on the other hand. For patch interior and edge basis functions, this is a consequence of their local linear independence in Lemma 4.6 and the property in Lemma 4.9, without any requirement on the hierarchical mesh. For the set of vertex basis functions $\Phi^{\ell}_{\mathbf{x}^{(i)}}$, by the hypotheses there exists an active element $Q \in G^{\ell}_{\mathbf{x}^{(i)}} \cap \mathcal{Q}$. Then, from Lemma 4.7 the vertex functions in $\Phi^{\ell}_{\mathbf{x}^{(i)}}$ are linearly independent in Q, and by Lemma 4.8 their span and the span of all the other functions in Φ^{ℓ} have trivial intersection in Q, which gives property (P1) with $D^{\ell}_i = Q$. □

5.4 Refinement algorithm

Theorem 5.2 gives us the only requirement for the linear independence of the hierarchical C^1 spline functions: active vertex functions must contain in its support an active element of the same level which is adjacent to the corresponding vertex. We now present a refinement algorithm that guarantees that this property is always satisfied.

Let us first define the set of elements in the hierarchical mesh adjacent to any vertex

$$G_\chi = \bigcup_{\ell=0}^{N-1} \Big(\bigcup_{i \in \mathcal{I}_\chi} G^\ell_{\mathbf{x}^{(i)}} \cap \mathcal{Q} \Big).$$

Then, for each element adjacent to a vertex, $Q \in G_\chi \cap G^\ell_{\mathbf{x}^{(i)}}$ for some $i \in \mathcal{I}_\chi$ and $\ell \in \{0, \dots, N-1\}$, and such that $Q \subset \Omega^{(i_m)}$ for some $m = 0, \dots \nu_i - 1$, we define the vertex-patch neighborhood

$$\mathcal{N}_\chi(Q) = \{Q' \in G^\ell \cap \mathcal{Q} : Q' \subset \Omega^{(i_m)} \cap \operatorname{supp} \phi, \text{ for } \phi \in \Phi^\ell_{\mathbf{x}^{(i)}}\} \setminus Q,$$

formed by the elements of level ℓ contained in $\Omega^{(i_m)}$ and in the support of vertex functions of level ℓ associated to $\mathbf{x}^{(i)}$. The marking algorithm proposed in Algorithm 1 enforces that whenever an element adjacent to a vertex is marked for refinement, the elements in its vertex-patch neighborhood are also marked, see also Figure 6.

Algorithm 1 `MARK_VERTEX-PATCH` $(\mathcal{Q}, \mathcal{M})$

Input: hierarchical mesh $\mathcal{Q}$, marked elements $\mathcal{M} \subseteq \mathcal{Q}$

set $\mathcal{V} = \bigcup_{Q \in \mathcal{M} \cap G_\chi} \mathcal{N}_\chi(Q) \setminus \mathcal{M}$

set $\mathcal{M} = \mathcal{M} \cup \mathcal{V}$

Output: updated set of marked elements $\mathcal{M}$

Remark 5.3. *If the initial mesh is very coarse one should also check whether marking the vertex-patch $\mathcal{N}_\chi(Q)$ marks any element adjacent to another vertex. This would force to mark also the vertex-patch neighborhood of that element, finally propagating the marking to all the boundary elements of the patch. To avoid this check, and to simplify the algorithm, we assume that the coarsest mesh is not coarser than 4×4 elements per patch, that is $k \geq 3$ inner knots, which prevents this situation to happen.*

The modification in the algorithm to mark the vertex-patch neighborhood can be easily combined with admissible refinement as introduced in [14], allowing to construct admissible hierarchical meshes such that the constraint on Theorem 5.2 is also satisfied. We recall that a mesh is admissible of class $\mu > 1$, if for any element of the hierarchical mesh the non-vanishing functions belong to at most μ different levels [14]. Depending on whether we look for admissibility with hierarchical splines or with truncated hierarchical splines, we respectively define, for an element $Q \in \mathcal{Q} \cap G^\ell$ of level $\ell \geq 0$, its $\mathcal{H}$-neighborhood and $\mathcal{T}$-neighborhood as

$$\mathcal{N}_\mathcal{H}(Q, \mu) = \{Q' \in \mathcal{Q} \cap G^{\ell-\mu+1} : Q' \cap S_{\text{ext}}(Q, \ell - \mu + 1) \neq \emptyset\},$$
$$\mathcal{N}_\mathcal{T}(Q, \mu) = \{Q' \in \mathcal{Q} \cap G^{\ell-\mu+1} : Q' \cap S_{\text{ext}}(Q, \ell - \mu + 2) \neq \emptyset\},$$

for $\ell - \mu + 1 > 0$, and $\mathcal{N}_\mathcal{H}(Q, \mu) = \mathcal{N}_\mathcal{T}(Q, \mu) = \emptyset$ if $\ell - \mu + 1 < 0$, see [13, Section 4.1]. In the definition, the multi-level support extension $S_{\text{ext}}(Q, k)$ is defined as the union of the supports of all basis functions of level k that do not vanish on Q, namely

$$S_{\text{ext}}(Q, k) = \bigcup \{\operatorname{supp} \phi : \phi \in \Phi^k \wedge Q \cap \operatorname{supp} \phi \neq \emptyset\}.$$

Using a generic notation $\mathcal{N}(Q, \mu)$ for both neighborhoods, and with the convention that $\mathcal{N}(Q, 0) = \emptyset$ for non-admissible meshes, the refinement algorithm in Algorithm 2 guarantees both the linear independence of the hierarchical basis and the admissibility of the adaptive mesh.

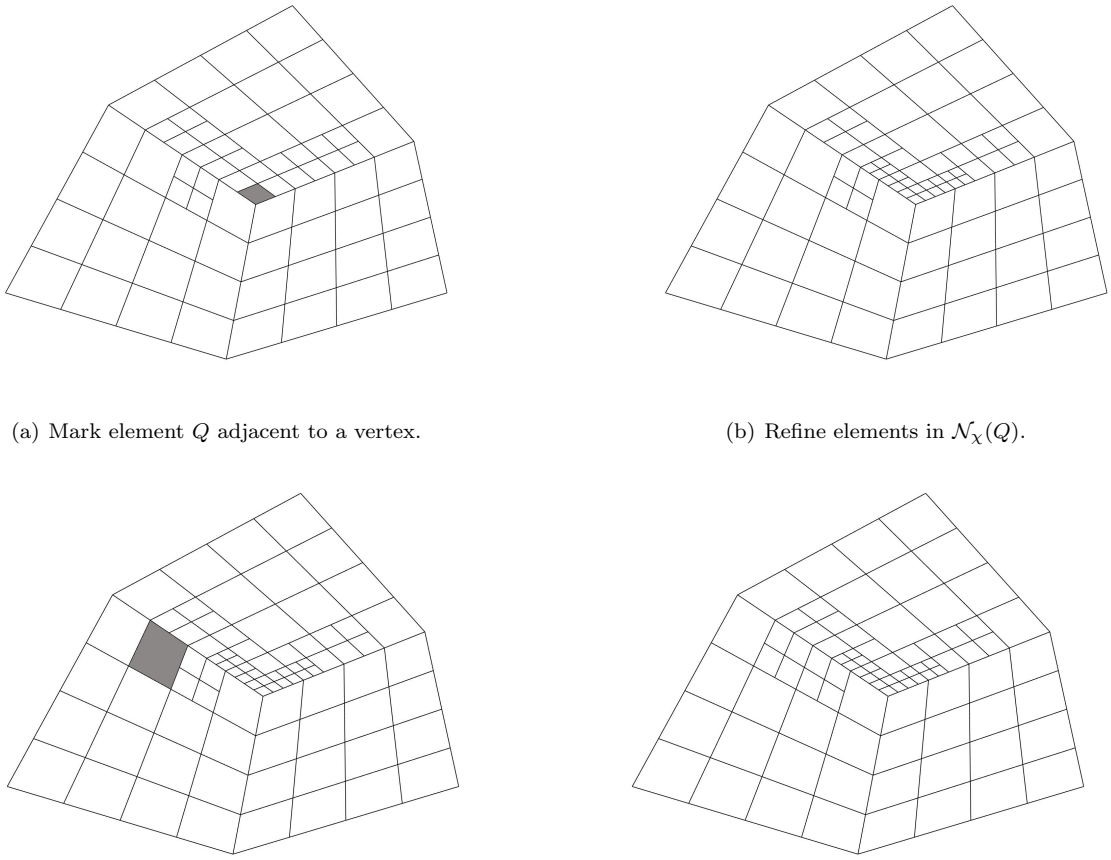

(a) Mark element Q adjacent to a vertex.

(b) Refine elements in $\mathcal{N}_\chi(Q)$.

(c) Mark element Q not adjacent to any vertex.

(d) Refine Q without additional refinement.

Figure 6: When one element Q adjacent to a vertex is marked, highlighted in dark grey in (a), all the elements in $\mathcal{N}_\chi(Q)$ are also refined (b). If the marked element Q is not adjacent to any vertex (c), no other elements need to be refined (d), even if Q belongs to the support of vertex basis functions.

Algorithm 2 `REFINE`$(\mathcal{Q}, \mathcal{M}, \mu)$, refine guaranteeing linear independence and admissibility

Input: admissible hierarchical mesh $\mathcal{Q}$, marked elements $\mathcal{M} \subseteq \mathcal{Q}$, admissible class μ
repeat
  set $\mathcal{M} =$ `MARK_VERTEX-PATCH` $(\mathcal{Q}, \mathcal{M})$
  set $\mathcal{U} = \bigcup_{Q \in \mathcal{M}} \mathcal{N}(Q, \mu) \setminus \mathcal{M}$
  set $\mathcal{M} = \mathcal{M} \cup \mathcal{U}$
until $\mathcal{U} = \emptyset$
update $\mathcal{Q}$ by replacing the elements in $\mathcal{M}$ by their children
Output: refined admissible mesh $\mathcal{Q}$

For any marked element the recursive refinement of its neighborhood guarantees the admissibility of the refined mesh as in [14]. If the marked element is adjacent to a vertex the marking of any other element in its vertex-patch neighborhood guarantees to satisfy the hypotheses of Theorem 5.2 and, consequently, the linear independence of the (truncated) hierarchical functions.

Theorem 5.4. *Assuming that we start from a coarse mesh G^0 with at least 4×4 elements per patch, and applying successive refinement with Algorithm 2, the construction of hierarchical C^1 splines gives a set $\mathcal{H}_{\mathbb{A}}$ or $\mathcal{T}_{\mathbb{A}}$ of linearly independent functions. Moreover, if $\mu > 1$ the mesh constructed in Algorithm 2 is admissible.*

5.5 Linear complexity of the refinement algorithm

We now prove a complexity estimate for the refinement algorithm, in the spirit of [7, 52], by following the analysis presented in [16] for the single-patch case.

We first remark that, thanks to the regularity assumptions on the parameterizations $\mathbf{F}^{(i)}$ made in Section 3.1.2, there exist two positive constants $c_{\mathbf{F}}, C_{\mathbf{F}} > 0$ such that

$$c_{\mathbf{F}} \leq |\det(\nabla \mathbf{F}^{(i)})(\xi_1, \xi_2)| \leq C_{\mathbf{F}}, \quad \text{for } (\xi_1, \xi_2) \in [0,1]^2,\ i \in \mathcal{I}_\Omega. \tag{31}$$

Since the knot vectors give uniform meshes in the parametric domain, the previous inequalities imply that for any element of level ℓ it holds that

$$\operatorname{diam}(Q) \simeq 2^{-\ell} \quad \text{for } Q \in G^\ell, \text{ and } \ell \geq 0, \tag{32}$$

where the hidden constants depend on $c_{\mathbf{F}}$ and $C_{\mathbf{F}}$, and also on the mesh size of the coarsest mesh G^0.

Next, we bound the distance of an element to other elements on its neighborhood. Given two elements Q, Q', we define the distance $\operatorname{dist}(Q, Q')$ as the Euclidean distance between their midpoints, understood as the image in their corresponding patches $\Omega^{(i)}, \Omega^{(i')}$ of their midpoints in the parametric domain $(0,1)^2$. Then, given an $\mathcal{H}$-admissible hierarchical mesh $\mathcal{Q}$, an element $Q \in \mathcal{Q} \cap G^\ell$ and $Q' \in \mathcal{N}_{\mathcal{H}}(\mathcal{Q}, Q, \mu)$, it holds that

$$\operatorname{dist}(Q, Q') \lesssim \operatorname{diam}(S_{\text{ext}}(Q, \ell - \mu + 1)) \leq 2^{-\ell} C_{\mathcal{N}},$$

where we have used (32) and the maximal support of C^1 basis functions as depicted in Figure 3. Therefore the constant $C_{\mathcal{N}}$ depends on the constants in (32), and through the supports it also depends on p, μ, r, and on $\nu = \max_{i \in \mathcal{I}_\chi} \nu_i$, the maximal valence of the vertices of the geometry. In a completely analogous fashion, given a $\mathcal{T}$-admissible hierarchical mesh $\mathcal{Q}$, an element $Q \in \mathcal{Q} \cap G^\ell$ and $Q' \in \mathcal{N}_{\mathcal{T}}(\mathcal{Q}, Q, \mu)$, it holds that

$$\operatorname{dist}(Q, Q') \lesssim \operatorname{diam}(S_{\text{ext}}(Q, \ell - \mu + 2)) \leq 2^{-\ell-1} C_{\mathcal{N}},$$

with the same dependencies as above, although truncation reduces the distance by a factor of 2. Note that the largest values of $C_{\mathcal{N}}$ occur for $\mu = 2$ and $r = p - 2$.

Similarly, given $Q \in G^\ell$ and $Q' \in \mathcal{N}_\chi(\mathcal{Q}, Q)$, using the support of vertex functions it also holds that

$$\operatorname{dist}(Q, Q') \leq 2^{-\ell-1} C_{\mathcal{N}_\chi},$$

where $C_{\mathcal{N}_\chi}$ depends on p, r and the constants in (32), the worst case being again $r = p - 2$.

The following lemma adapts the result of [16, Lemma 12] to the hierarchical multi-patch configuration here considered.

Lemma 5.5. *Let $\mathcal{Q}$ be an admissible mesh of class $\mu \geq 2$ satisfying the assumptions on Theorem 5.2, $Q' \in \mathcal{Q}$, and $\mathcal{Q}^* = \texttt{REFINE}(\mathcal{Q}, \{Q'\}, \mu)$ the mesh given by Algorithm 2 when marking only Q'. Then, for any element $Q \in \mathcal{Q}^* \setminus \mathcal{Q}$ it holds that*

$$\operatorname{dist}(Q, Q') \leq 2^{-\ell(Q)} C_{\text{dist}},$$

where $C_{\text{dist}} = \dfrac{C_{\mathcal{N}_\chi} + C_{\mathcal{N}}}{1 - 2^{1-\mu}}$ for $\mathcal{T}$-admissible meshes and $C_{\text{dist}} = \dfrac{C_{\mathcal{N}_\chi} + 2C_{\mathcal{N}}}{1 - 2^{1-\mu}}$ for $\mathcal{H}$-admissible meshes.

Proof. Let us assume that $\mathcal{Q}$ and $\mathcal{Q}^*$ are obtained by $\mathcal{T}$-admissible refinement, the case of $\mathcal{H}$-admissible refinement is proved analogously. Since Q is activated from applying Algorithm 2, there exists a sequence of elements $Q' = Q_J, Q_{J-1}, \ldots, Q_0$, such that Q is a child of Q_0, and for each $j = 1, \ldots, J$ either

$$Q_{j-1} \in \mathcal{N}_{\mathcal{T}}(\mathcal{Q}, Q_j, \mu) \quad \text{or} \quad Q_{j-1} \in \mathcal{N}_\chi(\mathcal{Q}, Q_j),$$

and moreover two markings of the second type, i.e., due to the vertex-patch neighborhood, do not appear consecutively. In the first case we have

$$\operatorname{dist}(Q_j, Q_{j-1}) \leq 2^{-\ell(Q_j)-1} C_{\mathcal{N}} \quad \text{and} \quad \ell(Q_{j-1}) = \ell(Q_j) - \mu + 1, \tag{33}$$

while the second case gives

$$\operatorname{dist}(Q_j, Q_{j-1}) \leq 2^{-\ell(Q_j)-1} C_{\mathcal{N}_\chi} \quad \text{and} \quad \ell(Q_{j-1}) = \ell(Q_j).$$

We trivially have that

$$\operatorname{dist}(Q, Q') \leq \operatorname{dist}(Q, Q_0) + \operatorname{dist}(Q_0, Q') \leq \operatorname{dist}(Q, Q_0) + \sum_{j=1}^{J} \operatorname{dist}(Q_j, Q_{j-1}),$$

and since Q is a child of Q_0 from dyadic refinement, we can bound the first term by $\operatorname{dist}(Q, Q_0) \lesssim 2^{-\ell(Q)}$.

For the sum, we know that two markings from the vertex-patch neighborhood do not appear consecutively, thus we can put ourselves in the worst case scenario, where the two types of marking alternate at every step. For simplicity, we can assume that J is even and, without loss of generality, that we mark the admissibility neighborhood at odd steps, and the vertex-patch neighborhood at even steps. We then have

$$\ell(Q_j) = \begin{cases} \ell(Q_0) + (\mu - 1)\,(j+1)/2 & \text{if } j \text{ is odd,} \\ \ell(Q_0) + (\mu - 1)\,j/2 & \text{if } j \text{ is even,} \end{cases}$$

from what we obtain

$$\begin{aligned} &\sum_{j=1}^{J} \operatorname{dist}(Q_j, Q_{j-1}) = \sum_{k=1}^{J/2} \left(\operatorname{dist}(Q_{2k}, Q_{2k-1}) + \operatorname{dist}(Q_{2k-1}, Q_{2k-2})\right) \\ &\leq \sum_{k=1}^{J/2} \left(2^{-\ell(Q_{2k})-1} C_{\mathcal{N}_\chi} + 2^{-\ell(Q_{2k-1})-1} C_{\mathcal{N}}\right) = \sum_{k=1}^{J/2} 2^{-\ell(Q_0)-1-k(\mu-1)} (C_{\mathcal{N}_\chi} + C_{\mathcal{N}}) \\ &< 2^{-\ell(Q_0)-1} (C_{\mathcal{N}_\chi} + C_{\mathcal{N}}) \sum_{k=0}^{\infty} 2^{-k(\mu-1)} = \frac{2^{-\ell(Q)}}{1 - 2^{1-\mu}} (C_{\mathcal{N}_\chi} + C_{\mathcal{N}}), \end{aligned}$$

where in the last step we have used that Q is a child of Q_0, and the same arguments as in [16]. The proof for the $\mathcal{H}$-admissible case is completely analogous, replacing the $\mathcal{N}_{\mathcal{T}}$ neighborhood by the $\mathcal{N}_{\mathcal{H}}$ neighborhood, and consequently the constant $C_{\mathcal{N}}$ by $2C_{\mathcal{N}}$ in (33). □

The following theorem states the linear complexity of the refinement algorithm, and generalizes the single-patch complexity estimates [16, Theorem 13] to the multi-patch case, see also [7, Theorem 2.4] and [52, Theorem 3.2].

Theorem 5.6. *Let $\mathcal{Q}_0 = G^0$ and $\mu \geq 2$, and let $\mathcal{Q}_0, \mathcal{Q}_1, \ldots, \mathcal{Q}_J$ the sequence of admissible meshes generated from the call to Algorithm 2, namely*

$$\mathcal{Q}_j = \texttt{REFINE}(\mathcal{Q}_{j-1}, \mathcal{M}_{j-1}, \mu), \quad \mathcal{M}_{j-1} \subseteq \mathcal{Q}_{j-1} \text{ for } j \in \{1, \ldots, J\}.$$

Then, there exists a positive constant Λ such that

$$\#\mathcal{Q}_J - \#\mathcal{Q}_0 \leq \Lambda \sum_{j=0}^{J-1} \#\mathcal{M}_j.$$

The constant Λ depends on p, r, μ, the constants on (32), the maximum valence ν and the type of admissible refinement.

Proof. The proof is completely analogous to the one in [16, Theorem 13], using the new estimate introduced in Lemma 5.5 in place of [16, Lemma 12]. The only difference is in the bound of the number of elements in the set

$$B(Q', j) = \{Q \in G^j : \operatorname{dist}(Q, Q') < 2^{1-j} C_{\text{dist}}\},$$

the set of elements of level $j \geq 0$ with distance to $Q' \in \mathcal{Q}$ smaller than $2^{1-j} C_{\text{dist}}$. A bound independent on Q' and j is easily proved using (31) and (32), the fact that the meshes in the parametric domain are uniform, and that refinement at every level is done by dyadic refinement. □

Remark 5.7. *It is very likely that one can remove the dependence on the constants in* (31)*, which appears through* (32)*, by using a different kind of proof, because the element neighborhoods may depend on how the patches glue together (the maximum valence), but are independent of the particular parameterizations* $\mathbf{F}^{(k)}$*. We have preferred to follow the proofs of previous papers, and maintain this dependence, for the sake of simplicity.*

6 Numerical tests

This section contains some numerical tests showing the application of the hierarchical C^1 spaces to adaptive isogeometric methods. In the examples, we consider both the Poisson problem and the biharmonic problem, where the adaptive refinement is automatically driven. The implementation is done based on the algorithms for hierarchical splines from [23], using the representation in terms of B-splines in Section 3.3 and the refinement mask in Section 5.2 for the evaluation and truncation of basis functions.

Our code is written in Matlab and is an extension of the one for the two-patch case [11], to which we refer for the details. The most important differences come from the need for local re-parameterizations, as already mentioned in Remark 3.1. These can be easily computed by arranging the control points in a two-dimensional array and applying simple changes in the directions of the array[1], and the same kind of arrangement should be applied to the indices of B-spline functions when computing the coefficients in Sections 3.3 and 5.2. Moreover, since every edge is attached to two vertices, the orientation of the edge in the vertex configuration may differ with respect to the one used for the definition of edge basis functions, in the sense that the relative position of two adjacent patches will change. In this case it is necessary, first, to correctly identify the five "extended" edge functions which are close to the vertex to compute the restricted matrices $\widehat{E}_{i_m,1}$ and $\widehat{E}_{i_{m+1},0}$ in Section 3.3, and second to take into account the sign change in the gluing data and the vectors $\mathbf{d}^{(i)}(\xi)$ and $\mathbf{t}^{(i)}(\xi)$ defined in Section 3.1.3, which also influences the sign of the last two columns of matrices $K_{i,m}$ and $K_{i,m+1}$.

6.1 Poisson problem

In the first two examples we consider the Poisson problem

$$\begin{cases} -\Delta u = f & \text{in } \Omega, \\ u = g & \text{on } \partial\Omega, \end{cases}$$

which we solve by an isogeometric algorithm based on the adaptive loop (see, e.g., [10])

$$\text{SOLVE} \longrightarrow \text{ESTIMATE} \longrightarrow \text{MARK} \longrightarrow \text{REFINE}. \tag{34}$$

More precisely, we *solve* the problem in its variational formulation imposing the Dirichlet boundary condition by Nitsche's method. Let us denote $\mathbb{W}_h = \operatorname{span}\{\mathcal{H}_{\mathbb{A}}\}$, we determine $u_h \in \mathbb{W}_h$ such that for all $v_h \in \mathbb{W}_h$

$$\int_\Omega \nabla u_h \cdot \nabla v_h - \int_{\Gamma_D} \frac{\partial u_h}{\partial \mathbf{n}} v_h - \int_{\Gamma_D} u_h \frac{\partial v_h}{\partial \mathbf{n}} + \int_{\Gamma_D} \frac{\gamma}{h_Q} u_h v_h = \int_\Omega f v_h - \int_{\Gamma_D} g \frac{\partial v_h}{\partial \mathbf{n}} + \int_{\Gamma_D} \frac{\gamma}{h_Q} g v_h,$$

[1] In Matlab, one can use the commands `fliplr`, `flipud` and `transpose`, or just consecutive uses of `rot90` if the Jacobian is assumed to be positive.

where h_Q is the local element size, and $\gamma = 10(p+1)$, with p being the degree, is the penalization term. The *error estimate* is computed with the residual-based estimator

$$\varepsilon^2(u_h) = \sum_{Q \in \mathcal{Q}} \varepsilon_Q^2(u_h), \quad \text{with} \quad \varepsilon_Q^2(u_h) = h_Q^2 \int_Q |f + \Delta u_h|^2.$$

The *marking* of the elements at each iteration is done using Dörfler's strategy. In the *refinement* step we apply Algorithm 2, and therefore we refine dyadically the marked elements, plus the ones necessary to guarantee linear independence and stability.

For both examples we report the results for degrees $p = 3, 4$ and 5, with regularity $r = p - 2$ and C^1 smoothness across the interfaces. We test the methods obtained by employing both the non-truncated and the truncated basis, and the refinement providing admissibility of class $\mu = 2, 3$. The goal is to show that using the C^1 space basis does not spoil the properties of the local refinement, and in particular the advantage over uniform refinement.

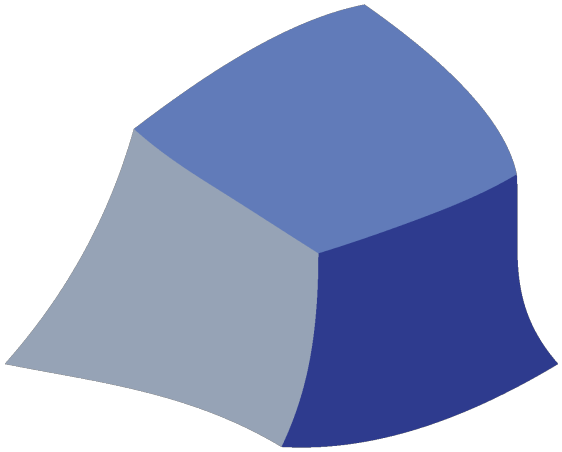

(a) Domain of Example 6.1.

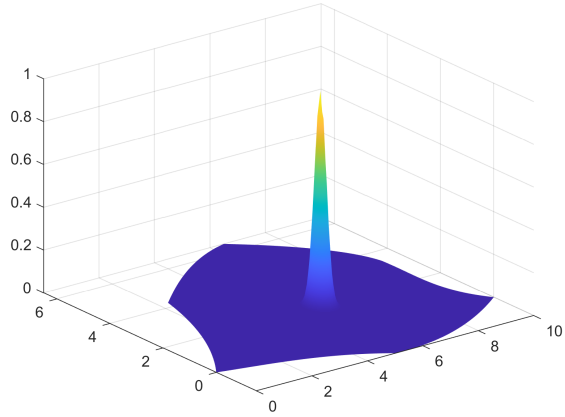

(b) Exact solution of Example 6.1.

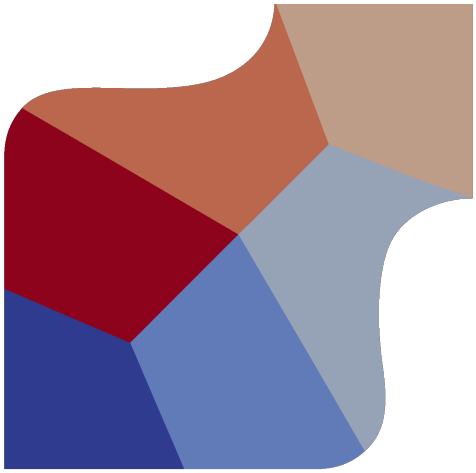

(c) Domain of Example 6.2.

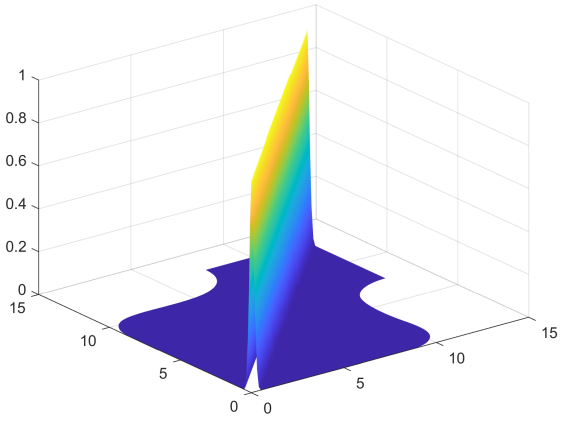

(d) Exact solution of Example 6.2.

Figure 7: Domains and exact solutions of Example 6.1 (top) and Example 6.2 (bottom).

Example 6.1. *For the first numerical example we consider the three-patch domain shown in Figure 7(a) which has been constructed in [37, Section 5] and possesses an analysis-suitable G^1 multi-patch parameterization. We study the Poisson problem with exact solution*

$$u(\mathbf{x}) = e^{-20(\|\mathbf{x}-\mathbf{P}\|^2)},$$

which is characterized by a peak at the point $\mathbf{P} = (17/3, 2)$, which coincides with the interior vertex of the geometry, see Figure 7(b).

The starting coarse mesh has 4×4 elements on each patch, and we use Dörfler's parameter equal to 0.80 for marking the elements. We run the adaptive method until the hierarchical space reaches nine levels. The behavior of the error in H^1 semi-norm with respect to the number of degrees of freedom (NDOF) is presented in Figure 8, where it is evident the advantage of using local refinement over the uniform one, regardless of the chosen basis and of the admissibility class. For higher degrees (see Figure 8, bottom), the refinement for the truncated basis tends to give smaller errors, but in all cases the optimal convergence rate is achieved.

In Figure 9 we show the meshes obtained for degree $p = 5$ after reaching six levels. As already observed in [10] for THB-splines, the refinement based on the truncated basis is more local than the one for the hierarchical basis, and a larger value of μ improves the locality of the refinement. The figure also shows how marking elements adjacent to the vertex extends the refinement to the elements in the vertex-patch neighborhood, but this does not affect the convergence rates.

Example 6.2. *In the second example, we consider the six-patch domain shown in Figure 7(c) with an analysis-suitable G^1 multi-patch parameterization taken from [35, Example 2], and the data of the problem are chosen such that the exact solution is*

$$u(x, y) = e^{-25(x-y)^2}.$$

This solution has a sharp ridge crossing the whole domain: in the middle part it coincides with two interfaces, while at the two endpoints it crosses two patches, see Figure 7(d). In this example the initial mesh has 6×6 elements on each patch, and we run the adaptive method with Dörfler's parameter equal to 0.75 until the hierarchical space reaches ten levels. The convergence results in Figure 10 (right) show, just like in the previous example, that in the three cases the error converges with optimal rate, and for higher degrees the refinement based on the truncated basis gives a slight advantage. In Figure 10 (left) we show the meshes obtained by applying the isogeometric method with degrees $p = 3, 4, 5$ for the truncated basis and admissibility class $\mu = 3$ when six hierarchical levels are reached. We see that the refinement concentrates along the diagonal in all cases, with some elements refined outside the diagonal due to the refinement of the vertex-patch neighborhood, but without affecting the convergence rate.

6.2 Biharmonic problem

For the final numerical test, we consider the biharmonic problem

$$\begin{cases} \Delta^2 u = f & \text{in } \Omega, \\ u = g_1 & \text{on } \partial\Omega, \\ \dfrac{\partial u}{\partial n} = g_2 & \text{on } \partial\Omega. \end{cases}$$

In order to solve the direct formulation of this problem with a Galerkin method, we need to use a discretization space of C^1 functions, and therefore in this case the C^1 hierarchical basis is a natural choice to define an adaptive isogeometric method. Let us denote $\mathbb{W}_h = \operatorname{span}\{\mathcal{H}_{\mathbb{A}}\}$ and $\mathbb{W}_{0,h} = \mathbb{W}_h \cap H_0^2(\Omega)$. The problem is to find $u_{0,h} \in \mathbb{W}_{0,h}$ such that for all $v_h \in \mathbb{W}_{0,h}$ it holds that

$$\int_\Omega \Delta u_{0,h} \Delta v_h = \int_\Omega f v_h - \int_\Omega \Delta u_{b,h} \Delta v_h,$$

where $u_{b,h} \in \mathbb{W}_h$ is a discrete function that satisfies the boundary conditions. The method is based on the same adaptive loop (34) we employed for the Poisson problem. To avoid the computation of third

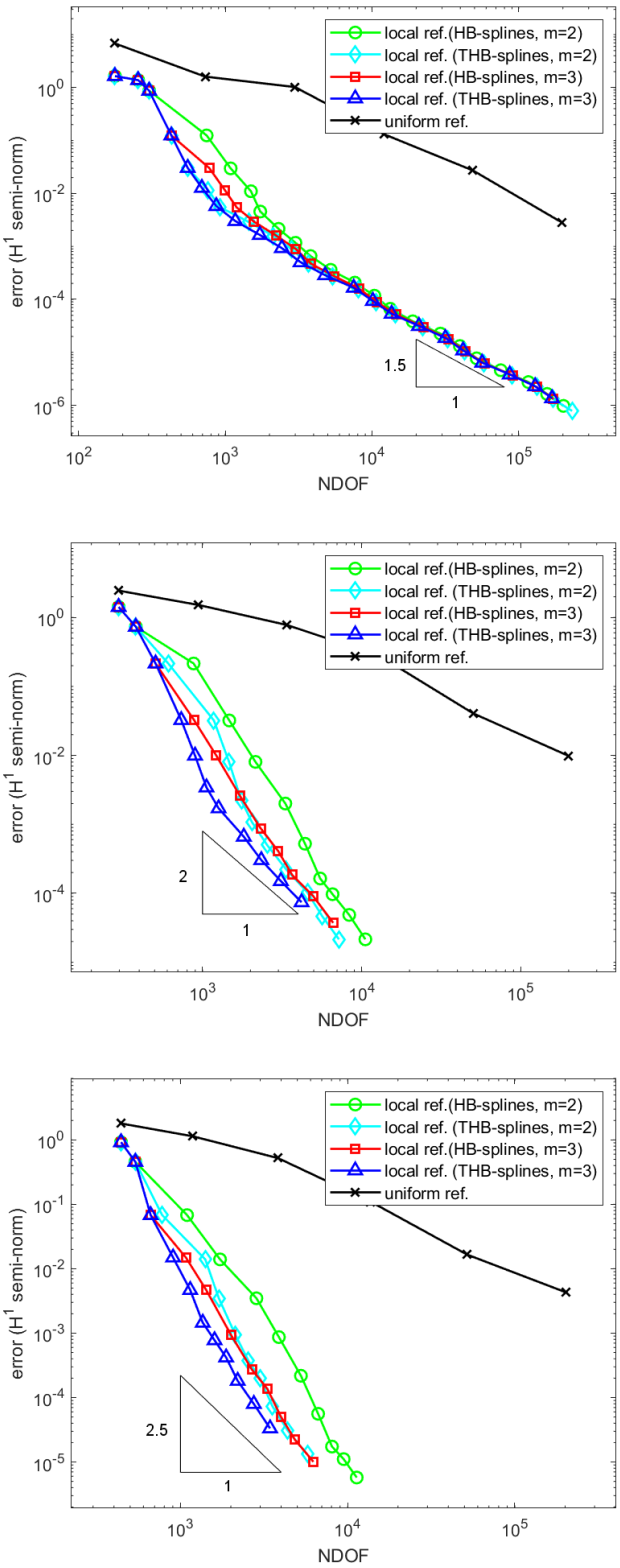

Figure 8: Example 6.1 (Poisson problem on a three-patch domain): convergence plots for degrees 3, 4 and 5 (from top to bottom) with admissibility $\mu = 2, 3$ in the refinement.

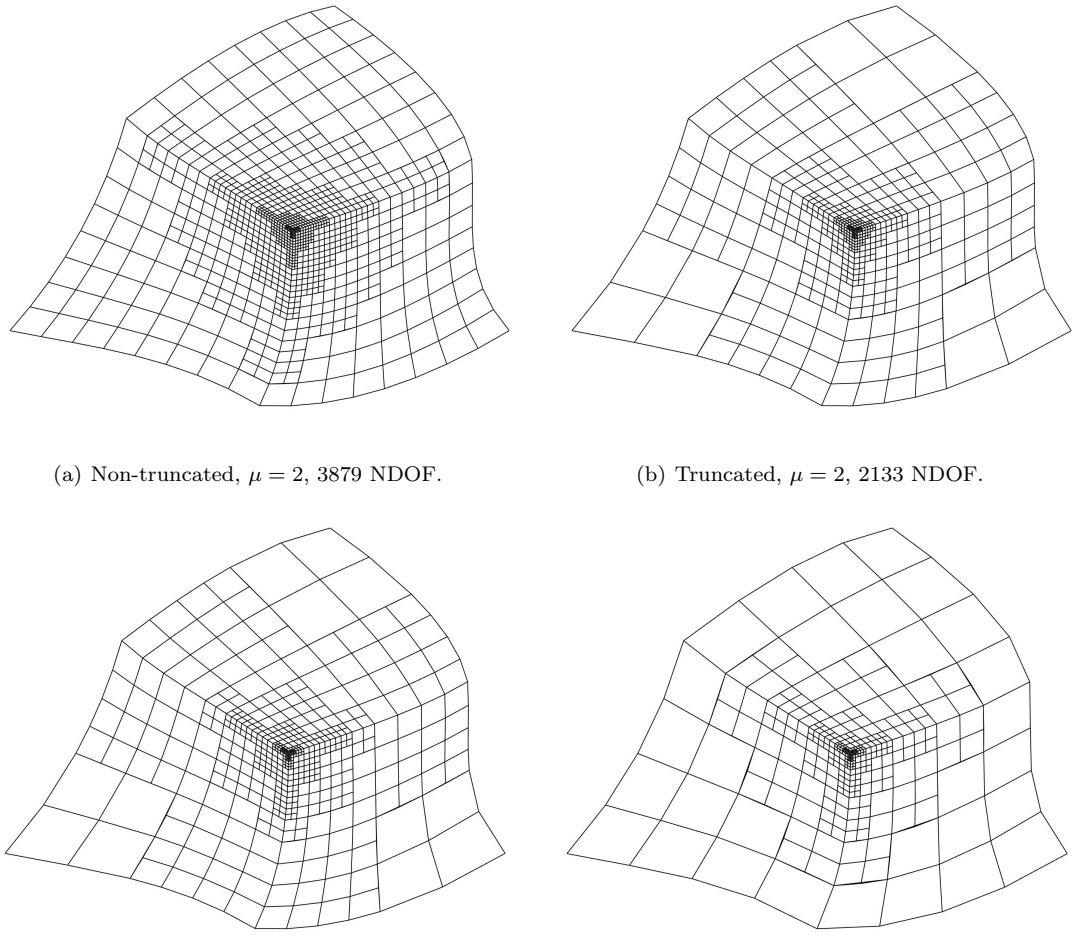

(a) Non-truncated, $\mu = 2$, 3879 NDOF.

(b) Truncated, $\mu = 2$, 2133 NDOF.

(c) Non-truncated, $\mu = 3$, 2001 NDOF.

(d) Truncated, $\mu = 3$, 1359 NDOF.

Figure 9: Example 6.1 (Poisson problem on a three-patch domain): six-level meshes obtained for degree 5.

and fourth order derivatives that would appear on Nitsche's method, the boundary conditions are imposed strongly through a projection into the space generated by boundary functions. For the same reason, instead of the residual error estimator we use the estimator presented in [1], which follows the original idea of [4], by enriching the space with C^1 bubble functions of degree $p+1$, and support on one single element. In particular, if we define the space of bubble functions $\mathbb{B}_h$, and define our solution as $u_h = u_{0,h} + u_{b,h}$, we compute an estimator of the error as the unique function $e_h \in \mathbb{B}_h$ such that for all $b_h \in \mathbb{B}_h$ it holds

$$\int_\Omega \Delta e_h \Delta b_h = \int_\Omega f b_h - \int_\Omega \Delta u_h \Delta b_h,$$

and an estimate of the error on each element $Q \in \mathcal{Q}$ is given by computing the energy norm $\|e_h\|_{E(Q)}$.

Example 6.3. *For the last numerical test we solve the biharmonic problem in the L-shaped domain composed of eight bilinearly parameterized patches as depicted in Figure 11(a), with exact solution, in polar coordinates* (ρ, θ)*, given by*

$$u(\rho, \theta) = \rho^{z+1}(C_1\, F_1(\theta) - C_2\, F_2(\theta)),$$

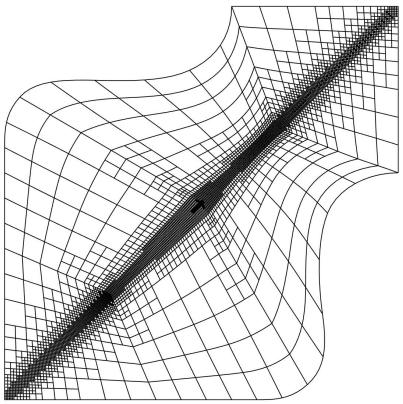

(a) 21240 NDOF.

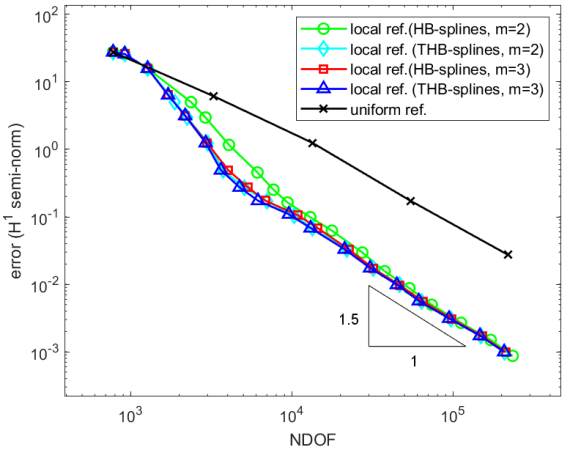

(b) Error for degree 3.

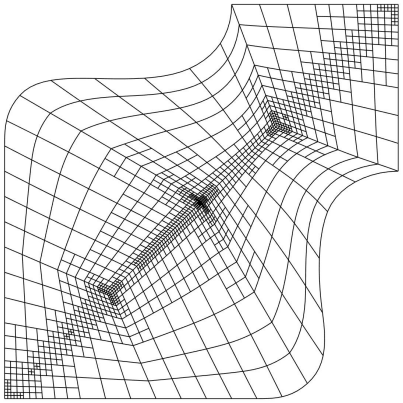

(c) 4855 NDOF

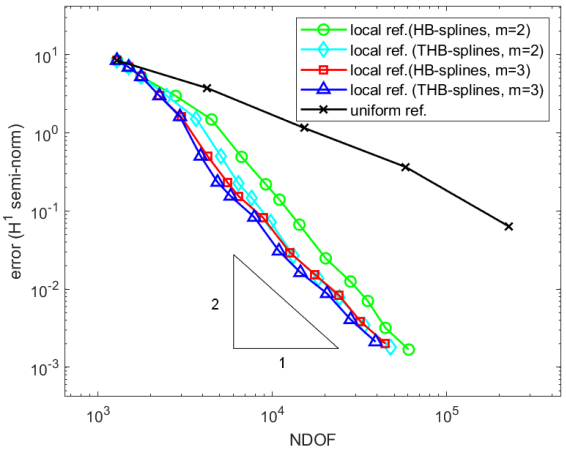

(d) Error for degree 4.

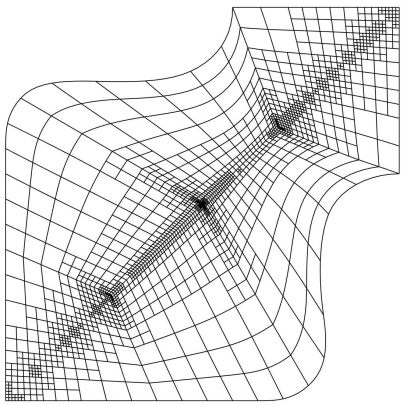

(e) 7104 NDOF.

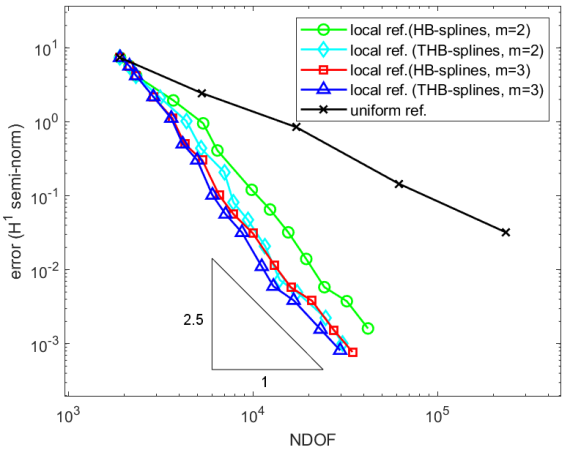

(f) Error for degree 5.

Figure 10: Example 6.2 (Poisson problem on a six-patch domain): six-level hierarchical meshes and convergence plots for degrees 3, 4 and 5 (from top to bottom) with admissibility $\mu = 2, 3$ in the refinement.

where

$$C_1 = \frac{1}{z-1}\sin\left(\frac{3(z-1)\pi}{2}\right) - \frac{1}{z-1}\sin\left(\frac{3(z+1)\pi}{2}\right),$$
$$C_2 = \cos\left(\frac{3(z-1)\pi}{2}\right) - \cos\left(\frac{3(z+1)\pi}{2}\right),$$
$$F_1(\theta) = \cos((z-1)\theta) - \cos((z+1)\theta),$$
$$F_2(\theta) = \frac{1}{z-1}\sin((z-1)\theta) - \frac{1}{z+1}\sin((z+1)\theta).$$

and $z = 0.544483736782464$*, that is, the smallest positive solution of*

$$\sin(z\omega) + z\sin(\omega) = 0,$$

with $\omega = 3\pi/2$ *for the L-shaped domain, see [28, Section 3.4]. It is well known that this solution has a singularity at the re-entrant corner. We present the results for degrees* $p = 3, 4, 5$*, with regularity* $r = p - 2$*, obtained by employing both the non-truncated and the truncated basis, with admissibility of class* $\mu = 3$*, and Dörfler parameter equal to* 0.80*.*

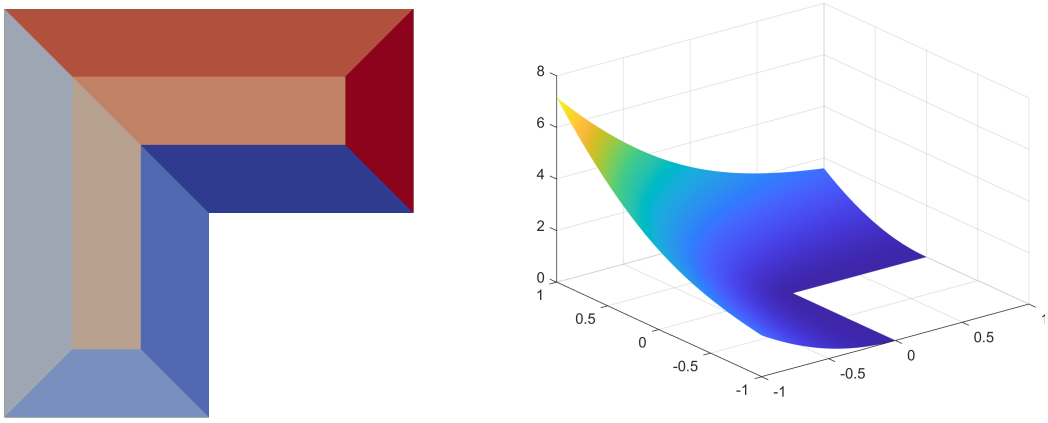

(a) Domain of Example 6.3

(b) Exact solution of Example 6.1

Figure 11: Domain and exact solution of Example 6.3.

In the test the initial mesh has 4×4 *elements on each patch, and we run the adaptive method until the hierarchical space reaches twelve levels. In Figure 12 (right), where we plot the obtained errors in* H^2 *semi-norm, it is clear the advantage of using local refinement over the uniform one, regardless of the employed basis. In the plot the convergence rate appears to be slightly better than the optimal one, which indicates that the asymptotic regime has not yet been reached, except for degree* $p = 3$*. In Figure 12 (left) we show the hierarchical meshes obtained when solving the problem with the truncated basis and stopping the iterations at six levels, and we see a similar behavior as for the other examples, with some elements refined away from the singularity for degree* $p = 5$ *but without affecting the convergence of the method.*

7 Conclusions

We developed an adaptive isogeometric method for solving PDEs over planar analysis-suitable G^1 multi-patch geometries with C^1 hierarchical splines. Since the C^1 spline spaces on one level lack local linear independence,

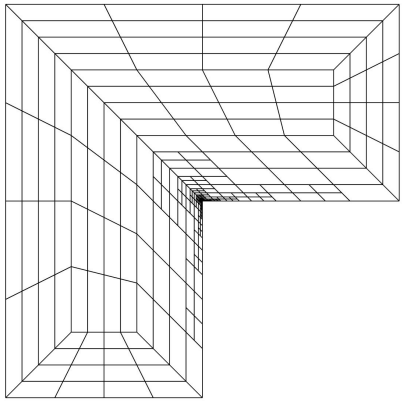

(a) 867 NDOF.

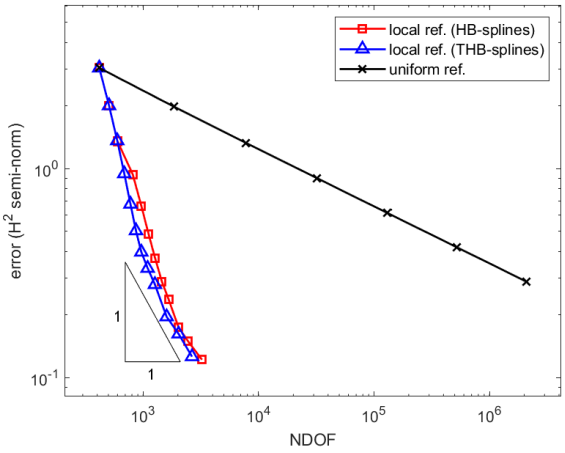

(b) Error for degree 3.

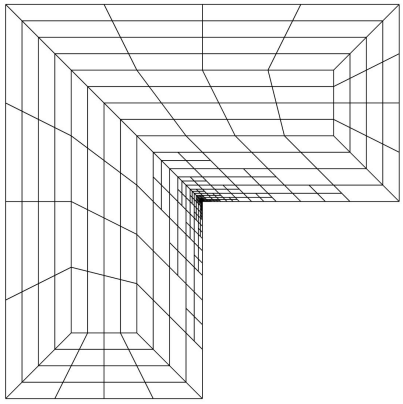

(c) 1081 NDOF.

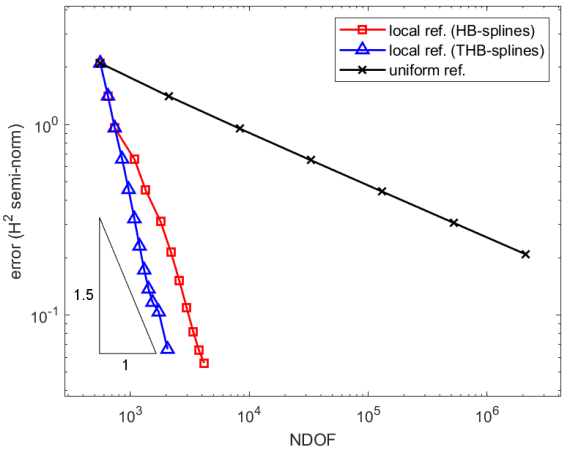

(d) Error for degree 4.

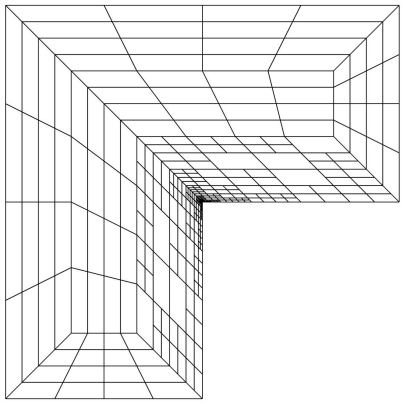

(e) 1433 NDOF.

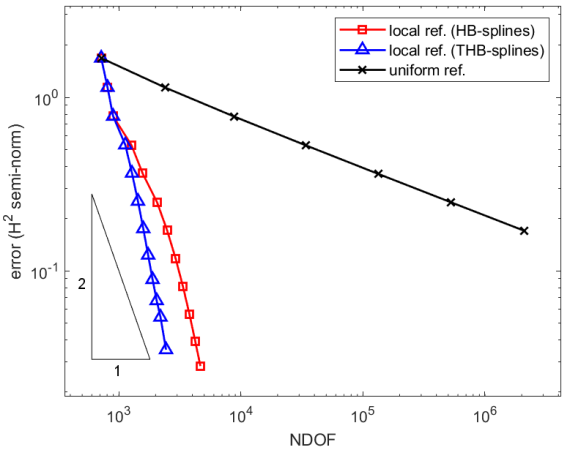

(f) Error for degree 5.

Figure 12: Example 6.1 (biharmonic problem on the L-shaped domain): six-level hierarchical meshes and convergence plots for degrees 3, 4 and 5 (from top to bottom).

as we demonstrated on the basis of an example, we analyzed the hierarchical spline construction under relaxed assumptions and proved that linear independence of the hierarchical basis can still be obtained.

The design of the adaptive method involved the investigation of several properties of the C^1 isogeometric spline space of each level, to guarantee that the relaxed assumptions are satisfied. This comprises its detailed characterization, the local linear independence of particular subsets of basis functions, as well as the refinement masks between two consecutive levels of refinement. In addition, we proved key properties of the resulting C^1 hierarchical spline space and its associated basis such as nestedness on refined meshes and, under a mild assumption on the mesh near the vertices, linear independence of the basis. We presented a refinement algorithm with linear complexity, which guarantees the construction of graded hierarchical meshes that fulfill the condition for linear independence. Finally, the potential of the adaptive scheme was demonstrated by solving the Poisson problem as well as the biharmonic problem over different planar analysis-suitable G^1 multi-patch parameterizations, where the numerical results indicated in all cases optimal convergence behavior.

In future work, we plan to extend our adaptive isogeometric spline method to the case of analysis-suitable G^1 multi-patch surfaces as well as to the application of further fourth order PDEs such as the Kirchhoff-Love shell problem [43]. From a more theoretical perspective, we plan to analyze the convergence properties of the adaptive method, for which it is first necessary to study the approximation properties of the (hierarchical) C^1 spline spaces.

A Definitions for the computation of C^1 basis functions

For the sake of completeness, we present in this appendix further definitions that are necessary to define and compute the basis functions of Section 3, and therefore also for the hierarchical basis.

A.1 Modified univariate basis functions

The modified basis functions $M^r_{j,p}$, for $j = 0, 1$, $M^{r+1}_{j,p}$, for $j = 0, 1, 2$, and $M^r_{j,p-1}$, for $j = 0, 1$, are given by

$$
\begin{aligned}
M^r_{0,p}(\xi) &= \sum_{j=0}^{1} N^r_{j,p}(\xi), & M^r_{1,p}(\xi) &= \frac{1}{p(k+1)} N^r_{1,p}(\xi),\\
M^{r+1}_{0,p}(\xi) &= \sum_{j=0}^{2} N^{r+1}_{j,p}(\xi), & M^{r+1}_{1,p}(\xi) &= \frac{1}{p(k+1)} \sum_{j=1}^{2} A(j) N^{r+1}_{j,p}(\xi),\\
M^{r+1}_{2,p}(\xi) &= \frac{B}{p(p-1)(k+1)^2} N^{r+1}_{2,p}(\xi),
\end{aligned}
$$

with $A(j) = j$ and $B = 1$ for $r < p-2$, and $A(j) = 2j-1$ and $B = 2$ for $r = p-2$, and

$$
M^r_{0,p-1}(\xi) = \sum_{j=0}^{1} N^r_{j,p-1}(\xi), \quad M^r_{1,p-1}(\xi) = \frac{1}{(p-1)(k+1)} N^r_{1,p-1}(\xi).
$$

A.2 Computation of gluing data

For analysis-suitable G^1 multi-patch parameterizations, the linear functions $\alpha^{(i,0)}$ and $\alpha^{(i,1)}$ and the quadratic function $\beta^{(i)}$ are uniquely determined up to a common function $\gamma^{(i)}$ (with $\gamma^{(i)}(\xi) \neq 0$) via

$$
\begin{aligned}
\alpha^{(i,0)}(\xi) &= \gamma^{(i)}(\xi) \det \begin{bmatrix} \partial_1 \mathbf{F}^{(i_0)}(0,\xi) & \partial_2 \mathbf{F}^{(i_0)}(0,\xi) \end{bmatrix},\\
\alpha^{(i,1)}(\xi) &= \gamma^{(i)}(\xi) \det \begin{bmatrix} \partial_1 \mathbf{F}^{(i_1)}(\xi,0) & \partial_2 \mathbf{F}^{(i_1)}(\xi,0) \end{bmatrix},\\
\beta^{(i)}(\xi) &= \gamma^{(i)}(\xi) \det \begin{bmatrix} \partial_2 \mathbf{F}^{(i_1)}(\xi,0) & \partial_1 \mathbf{F}^{(i_0)}(0,\xi) \end{bmatrix},
\end{aligned}
$$

and there always exist (non-unique) linear functions $\beta^{(i,0)}$ and $\beta^{(i,1)}$ such that (6) holds, see [20]. To uniquely determine the linear functions $\alpha^{(i,0)}$, $\alpha^{(i,1)}$, $\beta^{(i,0)}$ and $\beta^{(i,1)}$ for each inner edge $\Sigma^{(i)}$, we assume that they are selected by minimizing the terms

$$||\alpha^{(i,0)} - 1||^2_{L_2([0,1])} + ||\alpha^{(i,1)} - 1||^2_{L_2([0,1])}$$

and

$$||\beta^{(i,0)}||^2_{L_2([0,1])} + ||\beta^{(i,1)}||^2_{L_2([0,1])},$$

see [37]. For each boundary edge $\Sigma^{(i)}$, $i \in \mathcal{I}^{\Gamma}_{\Sigma}$, we can simply assign trivial functions $\alpha^{(i,0)} \equiv 1$ and $\beta^{(i,0)} \equiv 0$.

A.3 Functions involved in the definition of edge and vertex basis functions

The functions appearing in the definition of edge basis functions of Section 3.2.3 are given by

$$\begin{aligned} f^{(i,0)}_{(j_1,0)}(\xi_1,\xi_2) &= N^{r+1}_{j_1,p}(\xi_2) M^r_{0,p}(\xi_1) - \beta^{(i,0)}(\xi_2)(N^{r+1}_{j_1,p})'(\xi_2) M^r_{1,p}(\xi_1), \\ f^{(i,1)}_{(j_1,0)}(\xi_1,\xi_2) &= N^{r+1}_{j_1,p}(\xi_1) M^r_{0,p}(\xi_2) - \beta^{(i,1)}(\xi_1)(N^{r+1}_{j_1,p})'(\xi_1) M^r_{1,p}(\xi_2), \end{aligned} \tag{35}$$

and

$$\begin{aligned} f^{(i,0)}_{(j_1,1)}(\xi_1,\xi_2) &= \alpha^{(i,0)}(\xi_2) N^r_{j_1,p-1}(\xi_2) N^r_{1,p}(\xi_1), \\ f^{(i,1)}_{(j_1,1)}(\xi_1,\xi_2) &= -\alpha^{(i,1)}(\xi_1) N^r_{j_1,p-1}(\xi_1) N^r_{1,p}(\xi_2). \end{aligned} \tag{36}$$

Note that the expression is greatly simplified for boundary edges, first because only the patch i_0 must be considered, and second because one can use the values $\alpha^{(i,0)} \equiv 1$ and $\beta^{(i,0)} \equiv 0$.

The functions $g^{(i,m,\mathrm{prec})}_{\mathbf{j}}$ and $g^{(i,m,\mathrm{next})}_{\mathbf{j}}$, appearing in the definition of vertex basis functions of Section 3.2.4, are respectively given by

$$\begin{aligned} g^{(i,m,\mathrm{next})}_{\mathbf{j}}(\xi_1,\xi_2) = &\sum_{w=0}^{2} c^{(i_{m+1})}_{\mathbf{j},w} \left(M^{r+1}_{w,p}(\xi_2) M^r_{0,p}(\xi_1) - \beta^{(i_{m+1},0)}(\xi_2)(M^{r+1}_{w,p})'(\xi_2) M^r_{1,p}(\xi_1) \right) \\ &+ \sum_{w=0}^{1} d^{(i_{m+1})}_{\mathbf{j},w} \alpha^{(i_{m+1},0)}(\xi_2) M^r_{w,p-1}(\xi_2) M^r_{1,p}(\xi_1), \end{aligned} \tag{37}$$

$$\begin{aligned} g^{(i,m,\mathrm{prec})}_{\mathbf{j}}(\xi_1,\xi_2) = &\sum_{w=0}^{2} c^{(i_m)}_{\mathbf{j},w} \left(M^{r+1}_{w,p}(\xi_1) M^r_{0,p}(\xi_2) - \beta^{(i_m,1)}(\xi_1)(M^{r+1}_{w,p})'(\xi_1) M^r_{1,p}(\xi_2) \right) \\ &- \sum_{w=0}^{1} d^{(i_m)}_{\mathbf{j},w} \alpha^{(i_m,1)}(\xi_1) M^r_{w,p-1}(\xi_1) M^r_{1,p}(\xi_2), \end{aligned} \tag{38}$$

with the coefficients $c^{(k)}_{\mathbf{j},w}$ and $d^{(k)}_{\mathbf{j},w}$, for $k = i_m, i_{m+1}$, given by

$$c^{(k)}_{\mathbf{j},0} = \delta^{j_1}_0 \delta^{j_2}_0, \quad c^{(k)}_{\mathbf{j},1} = \mathbf{b}^{\delta}_{\mathbf{j}} \cdot \mathbf{t}^{(k)}(0), \quad c^{(k)}_{\mathbf{j},2} = (\mathbf{t}^{(k)}(0))^T \, A^{\delta}_{\mathbf{j}} \, \mathbf{t}^{(k)}(0) + \mathbf{b}^{\delta}_{\mathbf{j}} \cdot (\mathbf{t}^{(k)})'(0),$$

$$d^{(k)}_{\mathbf{j},0} = \mathbf{b}^{\delta}_{\mathbf{j}} \cdot \mathbf{d}^{(k)}(0), \quad d^{(k)}_{\mathbf{j},1} = (\mathbf{t}^{(k)}(0))^T \, A^{\delta}_{\mathbf{j}} \, \mathbf{d}^{(k)}(0) + \mathbf{b}^{\delta}_{\mathbf{j}} \cdot (\mathbf{d}^{(k)})'(0),$$

and for each $\mathbf{j} \in \mathbf{J}_{\chi}$ we use the auxiliary matrix and vector

$$A^{\delta}_{\mathbf{j}} = \begin{pmatrix} \delta^{j_1}_2 \delta^{j_2}_0 & \delta^{j_1}_1 \delta^{j_2}_1 \\ \delta^{j_1}_1 \delta^{j_2}_1 & \delta^{j_1}_0 \delta^{j_2}_2 \end{pmatrix} \quad \text{and} \quad \mathbf{b}^{\delta}_{\mathbf{j}} = (\delta^{j_1}_1 \delta^{j_2}_0, \delta^{j_1}_0 \delta^{j_2}_1).$$

Denoting $\mathbf{w} = (w_1, w_2)$, the remaining function $h^{(i,m)}_{\mathbf{j}}$ is given by

$$h^{(i,m)}_{\mathbf{j}}(\xi_1,\xi_2) = \sum_{w_1=0}^{1} \sum_{w_2=0}^{1} e^{(i_m)}_{\mathbf{j},\mathbf{w}} M^r_{w_1,p}(\xi_1) M^r_{w_2,p}(\xi_2), \tag{39}$$

with the coefficients $e^{(i_m)}_{\mathbf{j},\mathbf{w}}$ defined as

$$e^{(i_m)}_{\mathbf{j},(0,0)} = \delta_0^{j_1}\delta_0^{j_2},\ e^{(i_m)}_{\mathbf{j},(1,0)} = \mathbf{b}^{\delta}_{\mathbf{j}} \cdot \mathbf{t}^{(i_m)}(0),\ e^{(i_m)}_{\mathbf{j},(0,1)} = \mathbf{b}^{\delta}_{\mathbf{j}} \cdot \mathbf{t}^{(i_{m+1})}(0),$$

$$e^{(i_m)}_{\mathbf{j},(1,1)} = (\mathbf{t}^{(i_m)}(0))^T\ A^{\delta}_{\mathbf{j}}\ \mathbf{t}^{(i_{m+1})}(0) + \mathbf{b}^{\delta}_{\mathbf{j}} \cdot \partial_1\partial_2\mathbf{F}^{(i_m)}(0,0).$$

Note that $e^{(i_m)}_{\mathbf{j},(0,0)} = c^{(i_m)}_{\mathbf{j},0} = c^{(i_{m+1})}_{\mathbf{j},0}$, and that $e^{(i_m)}_{\mathbf{j},(1,0)} = c^{(i_m)}_{\mathbf{j},1}$ and $e^{(i_m)}_{\mathbf{j},(0,1)} = c^{(i_{m+1})}_{\mathbf{j},1}$.

A.4 Computation of matrices for representation in terms of B-splines

By replacing the modified basis functions with their definitions from Appendix A.1 in the expressions (37), and putting in evidence the expression of the edge functions in (35) and (36), we obtain the explicit representation of $g^{(i,m,\mathrm{prec})}_{\mathbf{j}}$ in terms of B-splines:

$$\begin{aligned}
g^{(i,m,\mathrm{prec})}_{\mathbf{j}}(\xi_1,\xi_2) &= c^{(i_m)}_{\mathbf{j},0}\left(\sum_{j=0}^{2} N^{r+1}_{j,p}(\xi_1)M^r_{0,p}(\xi_2) - \beta^{(i_m,1)}(\xi_1)(N^{r+1}_{j,p})'(\xi_1)M^r_{1,p}(\xi_2)\right)\\
&+ \frac{c^{(i_m)}_{\mathbf{j},1}}{p(k+1)}\left(\sum_{j=1}^{2} A(j)\left(N^{r+1}_{j,p}(\xi_1)M^r_{0,p}(\xi_2) - \beta^{(i_m,1)}(\xi_1)(N^{r+1}_{j,p})'(\xi_1)M^r_{1,p}(\xi_2)\right)\right)\\
&+ \frac{Bc^{(i_m)}_{\mathbf{j},2}}{p(p-1)(k+1)^2}\left(N^{r+1}_{2,p}(\xi_1)M^r_{0,p}(\xi_2) - \beta^{(i_m,1)}(\xi_1)(N^{r+1}_{2,p})'(\xi_1)M^r_{1,p}(\xi_2)\right)\\
&- \frac{d^{(i_m)}_{\mathbf{j},0}}{p(k+1)}\sum_{j=0}^{1}\alpha^{(i_m,1)}(\xi_1)N^r_{j,p-1}(\xi_1)N^r_{1,p}(\xi_2) - \frac{d^{(i_m)}_{\mathbf{j},1}}{p(p-1)(k+1)^2}\alpha^{(i_m,1)}(\xi_1)N^r_{1,p-1}(\xi_1)N^r_{1,p}(\xi_2)\\
&= c^{(i_m)}_{\mathbf{j},0}\sum_{j=0}^{2} f^{(i_m,1)}_{(j,0)}(\xi_1,\xi_2) + \frac{c^{(i_m)}_{\mathbf{j},1}}{p(k+1)}\sum_{j=1}^{2} A(j) f^{(i_m,1)}_{(j,0)}(\xi_1,\xi_2)\\
&+ \frac{Bc^{(i_m)}_{\mathbf{j},2}}{p(p-1)(k+1)^2} f^{(i_m,1)}_{(2,0)}(\xi_1,\xi_2) + \frac{d^{(i_m)}_{\mathbf{j},0}}{p(k+1)}\sum_{j=0}^{1} f^{(i_m,1)}_{(j,1)}(\xi_1,\xi_2) + \frac{d^{(i_m)}_{\mathbf{j},1}}{p(p-1)(k+1)^2} f^{(i_m,1)}_{(1,1)}(\xi_1,\xi_2)\\
&= c^{(i_m)}_{\mathbf{j},0} f^{(i_m,1)}_{(0,0)}(\xi_1,\xi_2) + \left(c^{(i_m)}_{\mathbf{j},0} + \frac{A(1)c^{(i_m)}_{\mathbf{j},1}}{p(k+1)}\right) f^{(i_m,1)}_{(1,0)}(\xi_1,\xi_2)\\
&+ \left(c^{(i_m)}_{\mathbf{j},0} + \frac{A(2)c^{(i_m)}_{\mathbf{j},1}}{p(k+1)} + \frac{Bc^{(i_m)}_{\mathbf{j},2}}{p(p-1)(k+1)^2}\right) f^{(i_m,1)}_{(2,0)}(\xi_1,\xi_2) + \frac{d^{(i_m)}_{\mathbf{j},0}}{p(k+1)} f^{(i_m,1)}_{(0,1)}(\xi_1,\xi_2)\\
&+ \left(\frac{d^{(i_m)}_{\mathbf{j},0}}{p(k+1)} + \frac{d^{(i_m)}_{\mathbf{j},1}}{p(p-1)(k+1)^2}\right) f^{(i_m,1)}_{(1,1)}(\xi_1,\xi_2).
\end{aligned}$$

In a completely analogous fashion, starting from (38) we obtain that

$$\begin{aligned}
g^{(i,m,\mathrm{next})}_{\mathbf{j}}(\xi_1,\xi_2) &= c^{(i_{m+1})}_{\mathbf{j},0} f^{(i_{m+1},0)}_{(0,0)}(\xi_1,\xi_2) + \left(c^{(i_{m+1})}_{\mathbf{j},0} + \frac{A(1)c^{(i_{m+1})}_{\mathbf{j},1}}{p(k+1)}\right) f^{(i_{m+1},0)}_{(1,0)}(\xi_1,\xi_2)\\
&+ \left(c^{(i_{m+1})}_{\mathbf{j},0} + \frac{A(2)c^{(i_{m+1})}_{\mathbf{j},1}}{p(k+1)} + \frac{Bc^{(i_{m+1})}_{\mathbf{j},2}}{p(p-1)(k+1)^2}\right) f^{(i_{m+1},0)}_{(2,0)}(\xi_1,\xi_2) + \frac{d^{(i_{m+1})}_{\mathbf{j},0}}{p(k+1)} f^{(i_{m+1},0)}_{(0,1)}(\xi_1,\xi_2)\\
&+ \left(\frac{d^{(i_{m+1})}_{\mathbf{j},0}}{p(k+1)} + \frac{d^{(i_{m+1})}_{\mathbf{j},1}}{p(p-1)(k+1)^2}\right) f^{(i_{m+1},0)}_{(1,1)}(\xi_1,\xi_2).
\end{aligned}$$

From these expressions we get the matrices $K_{i,m}$ and $K_{i,m+1}$ of Section 3.3, that we wrote there replacing $A(j)$ and B with their particular values for $r = p - 2$.

Similarly, replacing the expression of the modified univariate basis functions in (39), we have

$$
\begin{aligned}
h_{\mathbf{j}}^{(i,m)}(\xi_1,\xi_2) &= \sum_{w_1=0}^{1}\sum_{w_2=0}^{1} e_{\mathbf{j},\mathbf{w}}^{(i_m)} M_{w_1,p}^r(\xi_1) M_{w_2,p}^r(\xi_2) \\
&= e_{\mathbf{j},(0,0)}^{(i_m)} \sum_{j=0}^{1} N_{j,p}^r(\xi_1) \sum_{j=0}^{1} N_{j,p}^r(\xi_2) + \frac{e_{\mathbf{j},(1,0)}^{(i_m)}}{p(k+1)} N_{1,p}^r(\xi_1) \sum_{j=0}^{1} N_{j,p}^r(\xi_2) \\
&+ \frac{e_{\mathbf{j},(0,1)}^{(i_m)}}{p(k+1)} \sum_{j=0}^{1} N_{j,p}^r(\xi_1) N_{1,p}^r(\xi_2) + \frac{e_{\mathbf{j},(1,1)}^{(i_m)}}{p^2(k+1)^2} N_{1,p}^r(\xi_1) N_{1,p}^r(\xi_2) \\
&= e_{\mathbf{j},(0,0)}^{(i_m)} N_{0,p}^r(\xi_1) N_{0,p}^r(\xi_2) + \left(e_{\mathbf{j},(0,0)}^{(i_m)} + \frac{e_{\mathbf{j},(1,0)}^{(i_m)}}{p(k+1)} \right) N_{1,p}^r(\xi_1) N_{0,p}^r(\xi_2) \\
&+ \left(e_{\mathbf{j},(0,0)}^{(i_m)} + \frac{e_{\mathbf{j},(0,1)}^{(i_m)}}{p(k+1)} \right) N_{0,p}^r(\xi_1) N_{1,p}^r(\xi_2) \\
&+ \left(e_{\mathbf{j},(0,0)}^{(i_m)} + \frac{e_{\mathbf{j},(0,1)}^{(i_m)}}{p(k+1)} + \frac{e_{\mathbf{j},(1,0)}^{(i_m)}}{p(k+1)} + \frac{e_{\mathbf{j},(1,1)}^{(i_m)}}{p^2(k+1)^2} \right) N_{1,p}^r(\xi_1) N_{1,p}^r(\xi_2),
\end{aligned}
$$

from which we get, using the relations between $c_{\mathbf{j}}$ and $e_{\mathbf{j}}$ in Appendix A.3, the matrix $V_{i,m}$ of Section 3.3.

Acknowledgment

Mario Kapl has been partially supported by the Austrian Science Fund (FWF) through the project P 33023-N. Rafael Vázquez has been partially supported by the Swiss National Science Foundation via the project n.200021_188589 and by the ERC AdG project CHANGE n.694515. These supports are gratefully acknowledged. Cesare Bracco, Carlotta Giannelli and Rafael Vázquez are members of the INdAM research group GNCS. The INdAM support through GNCS and Finanziamenti Premiali SUNRISE is gratefully acknowledged.

References

[1] P. Antolin, A. Buffa, and L. Coradello. A hierarchical approach to the a posteriori error estimation of isogeometric Kirchhoff plates and Kirchhoff-Love shells. *Comput. Methods Appl. Mech. Engrg.*, 363:112919, 2020.

[2] A. Apostolatos, M. Breitenberger, R. Wüchner, and K.-U. Bletzinger. Domain decomposition methods and Kirchhoff-Love shell multipatch coupling in isogeometric analysis. In B. Jüttler and B. Simeon, editors, *Isogeometric Analysis and Applications 2014*, pages 73–101. Springer, 2015.

[3] F. Auricchio, L. Beirão da Veiga, A. Buffa, C. Lovadina, A. Reali, and G. Sangalli. A fully "locking-free" isogeometric approach for plane linear elasticity problems: a stream function formulation. *Comput. Methods Appl. Mech. Engrg.*, 197(1):160–172, 2007.

[4] R. E. Bank and R. K. Smith. A posteriori error estimates based on hierarchical bases. *SIAM J. Numer. Anal.*, 30(4):921–935, 1993.

[5] A. Benvenuti. *Isogeometric Analysis for C^1-continuous Mortar Method*. PhD thesis, Corso di Dottorato in Matematica e Statistica, Università degli Studi di Pavia, 2017.

[6] M. Bercovier and T. Matskewich. *Smooth Bézier Surfaces over Unstructured Quadrilateral Meshes*. Lecture Notes of the Unione Matematica Italiana, Springer, 2017.

[7] P. Binev, W. Dahmen, and R. DeVore. Adaptive finite element methods with convergence rates. *Numer. Math.*, 97(2):219–268, 2004.

[8] A. Blidia, B. Mourrain, and N. Villamizar. G^1-smooth splines on quad meshes with 4-split macro-patch elements. *Comput. Aided Geom. Des.*, 52-53:106 – 125, 2017.

[9] A. Blidia, B. Mourrain, and G. Xu. Geometrically smooth spline bases for data fitting and simulation. *Comput. Aided Geom. Des.*, 78:101814, 2020.

[10] C. Bracco, A. Buffa, C. Giannelli, and R. Vázquez. Adaptive isogeometric methods with hierarchical splines: an overview. *Discret. Contin. Dyn. S.*, 39(1):241–261, 2019.

[11] C. Bracco, C. Giannelli, M. Kapl, and R. Vázquez. Isogeometric analysis with C^1 hierarchical functions on planar two-patch geometries. *Comput. Math. Appl.*, 80(11):2538–2562, 2020.

[12] C. Bracco, C. Giannelli, and R Vázquez. Refinement algorithms for adaptive isogeometric methods with hierarchical splines. *Axioms*, 7(3):43, 2018.

[13] A. Buffa, G. Gantner, C. Giannelli, D. Praetorius, and R. Vázquez. Mathematical foundations of adaptive isogeometric analysis. *Arch. Comput. Methods. Engrg.* To appear. arXiv:2107.02023.

[14] A. Buffa and C. Giannelli. Adaptive isogeometric methods with hierarchical splines: Error estimator and convergence. *Math. Models Methods Appl. Sci.*, 26:1–25, 2016.

[15] A. Buffa and C. Giannelli. Adaptive isogeometric methods with hierarchical splines: Optimality and convergence rates. *Math. Models Methods Appl. Sci.*, 27:2781–2802, 2017.

[16] A. Buffa, C. Giannelli, P. Morgenstern, and D. Peterseim. Complexity of hierarchical refinement for a class of admissible mesh configurations. *Comput. Aided Geom. Design*, 47:83–92, 2016.

[17] H. Casquero, X. Wei, D. Toshniwal, A. Li, T. J. R. Hughes, J. Kiendl, and Y. J. Zhang. Seamless integration of design and Kirchhoff-Love shell analysis using analysis-suitable unstructured T-splines. *Comput. Methods Appl. Mech. Engrg.*, 360:112765, 2020.

[18] C.L. Chan, C. Anitescu, and T. Rabczuk. Isogeometric analysis with strong multipatch C^1-coupling. *Comput. Aided Geom. Des.*, 62:294–310, 2018.

[19] C.L. Chan, C. Anitescu, and T. Rabczuk. Strong multipatch C^1-coupling for isogeometric analysis on 2D and 3D domains. *Comput. Methods Appl. Mech. Engrg.*, 357:112599, 2019.

[20] A. Collin, G. Sangalli, and T. Takacs. Analysis-suitable G^1 multi-patch parametrizations for C^1 isogeometric spaces. *Comput. Aided Geom. Des.*, 47:93 – 113, 2016.

[21] L. Coradello, P. Antolin, R. Vázquez, and A. Buffa. Adaptive isogeometric analysis on two-dimensional trimmed domains based on a hierarchical approach. *Comput. Methods Appl. Mech. Engrg.*, 364:112925, 2020.

[22] G. Gantner, D. Haberlik, and D. Praetorius. Adaptive IGAFEM with optimal convergence rates: Hierarchical B-splines. *Math. Models Methods Appl. Sci.*, 27:2631–2674, 2017.

[23] E. Garau and R. Vázquez. Algorithms for the implementation of adaptive isogeometric methods using hierarchical B-splines. *Appl. Numer. Math.*, 123:58–87, 2018.

[24] C. Giannelli, B. Jüttler, , Stefan K. Kleiss, Angelos Mantzaflaris, Bernd Simeon, and Jaka Špeh. THB-splines: An effective mathematical technology for adaptive refinement in geometric design and isogeometric analysis. *Comput. Methods Appl. Mech. Engrg.*, 299:337–365, 2016.

[25] C. Giannelli, B. Jüttler, and H. Speleers. THB–splines: the truncated basis for hierarchical splines. *Comput. Aided Geom. Des.*, 29:485–498, 2012.

[26] C. Giannelli, B. Jüttler, and H. Speleers. Strongly stable bases for adaptively refined multilevel spline spaces. *Adv. Comp. Math.*, 40:459–490, 2014.

[27] H. Gómez, V. M Calo, Y. Bazilevs, and T. J. R. Hughes. Isogeometric analysis of the Cahn–Hilliard phase-field model. *Comput. Methods Appl. Mech. Engrg.*, 197(49):4333–4352, 2008.

[28] P. Grisvard. *Singularities in boundary value problems*, volume 22 of *Recherches en Mathématiques Appliquées [Research in Applied Mathematics]*. Masson, Paris; Springer-Verlag, Berlin, 1992.

[29] Y. Guo and M. Ruess. Nitsche's method for a coupling of isogeometric thin shells and blended shell structures. *Comp. Methods Appl. Mech. Engrg.*, 284:881–905, 2015.

[30] P. Hennig, M. Ambati, L. De Lorenzis, and M. Kästner. Projection and transfer operators in adaptive isogeometric analysis with hierarchical B-splines. *Comput. Methods Appl. Mech. Engrg.*, 334:313 – 336, 2018.

[31] P. Hennig, S. Müller, and M. Kästner. Bézier extraction and adaptive refinement of truncated hierarchical NURBS. *Comput. Methods Appl. Mech. Engrg.*, 305:316–339, 2016.

[32] T. J. R. Hughes, G. Sangalli, T. Takacs, and D. Toshniwal. Chapter 8 - Smooth multi-patch discretizations in Isogeometric Analysis. In *Geometric Partial Differential Equations - Part II*, volume 22 of *Handbook of Numerical Analysis*, pages 467–543. Elsevier, 2021.

[33] M. Kapl, F. Buchegger, M. Bercovier, and B. Jüttler. Isogeometric analysis with geometrically continuous functions on planar multi-patch geometries. *Comput. Methods Appl. Mech. Engrg.*, 316:209 – 234, 2017.

[34] M. Kapl, G. Sangalli, and T. Takacs. Dimension and basis construction for analysis-suitable G^1 two-patch parameterizations. *Comput. Aided Geom. Des.*, 52–53:75 – 89, 2017.

[35] M. Kapl, G. Sangalli, and T. Takacs. Construction of analysis-suitable G^1 planar multi-patch parameterizations. *Comput.-Aided Des.*, 97:41–55, 2018.

[36] M. Kapl, G. Sangalli, and T. Takacs. Isogeometric analysis with C^1 functions on unstructured quadrilateral meshes. *The SMAI journal of computational mathematics*, 5:67–86, 2019.

[37] M. Kapl, G. Sangalli, and T. Takacs. An isogeometric C^1 subspace on unstructured multi-patch planar domains. *Comput. Aided Geom. Des.*, 69:55–75, 2019.

[38] M. Kapl, G. Sangalli, and T. Takacs. A family of C^1 quadrilateral finite elements. *Adv. Comp. Math.*, 47(6):82, 2021.

[39] M. Kapl, V. Vitrih, B. Jüttler, and K. Birner. Isogeometric analysis with geometrically continuous functions on two-patch geometries. *Comput. Math. Appl.*, 70(7):1518 – 1538, 2015.

[40] K. Karčiauskas, T. Nguyen, and J. Peters. Generalizing bicubic splines for modeling and IGA with irregular layout. *Comput.-Aided Des.*, 70:23–35, 2016.

[41] K. Karčiauskas and J. Peters. Refinable G^1 functions on G^1 free-form surfaces. *Comput. Aided Geom. Des.*, 54:61–73, 2017.

[42] K. Karčiauskas and J. Peters. Refinable bi-quartics for design and analysis. *Comput.-Aided Des.*, 102:204–214, 2018.

[43] J. Kiendl, K.-U. Bletzinger, J. Linhard, and R. Wüchner. Isogeometric shell analysis with Kirchhoff-Love elements. *Comput. Methods Appl. Mech. Engrg.*, 198(49):3902–3914, 2009.

[44] G. Lorenzo, M. A. Scott, K. Tew, T. J. R. Hughes, and H. Gomez. Hierarchically refined and coarsened splines for moving interface problems, with particular application to phase-field models of prostate tumor growth. *Comput. Methods Appl. Mech. Engrg.*, 319:515–548, 2017.

[45] B. Mourrain, R. Vidunas, and N. Villamizar. Dimension and bases for geometrically continuous splines on surfaces of arbitrary topology. *Comput. Aided Geom. Des.*, 45:108 – 133, 2016.

[46] T. Nguyen, K. Karčiauskas, and J. Peters. A comparative study of several classical, discrete differential and isogeometric methods for solving Poisson's equation on the disk. *Axioms*, 3(2):280–299, 2014.

[47] T. Nguyen, K. Karčiauskas, and J. Peters. C^1 finite elements on non-tensor-product 2d and 3d manifolds. *Appl. Math. Comput.*, 272:148 – 158, 2016.

[48] T. Nguyen and J. Peters. Refinable C^1 spline elements for irregular quad layout. *Comput. Aided Geom. Des.*, 43:123 – 130, 2016.

[49] A. Riffnaller-Schiefer, U. H. Augsdörfer, and D.W. Fellner. Isogeometric shell analysis with NURBS compatible subdivision surfaces. *Appl. Math. Comput.*, 272:139–147, 2016.

[50] A. Sailer and B. Jüttler. Approximately C^1-smooth isogeometric functions on two-patch domains. In *Isogeometric Analysis and Applications 2018*, pages 157–175. Springer, LNCSE, 2021.

[51] M. A. Scott, R. N. Simpson, J. A. Evans, S. Lipton, S. P. A. Bordas, T. J. R. Hughes, and T. W. Sederberg. Isogeometric boundary element analysis using unstructured T-splines. *Comput. Methods Appl. Mech. Engrg.*, 254:197–221, 2013.

[52] R. Stevenson. Optimality of a standard adaptive finite element method. *Found. Comput. Math.*, 7(2):245–269, 2007.

[53] T. Takacs and D. Toshniwal. Almost-C^1 splines: Biquadratic splines on unstructured quadrilateral meshes and their application to fourth order problems. Technical Report 2201.11491, arXiv.org, 2022.

[54] D. Toshniwal, H. Speleers, and T. J. R. Hughes. Smooth cubic spline spaces on unstructured quadrilateral meshes with particular emphasis on extraordinary points: Geometric design and isogeometric analysis considerations. *Comput. Methods Appl. Mech. Engrg.*, 327:411–458, 2017.

[55] X. Wei. THU-splines: Highly localized refinement on smooth unstructured splines. Technical Report 2104.00090, arXiv.org, 2021.

[56] X. Wei, Y. Zhang, T. J. R. Hughes, and M. A. Scott. Truncated hierarchical Catmull-Clark subdivision with local refinement. *Comput. Methods Appl. Mech. Engrg.*, 291:1–20, 2015.

[57] X. Wei, Y. Zhang, L. Liu, and T. J. R. Hughes. Truncated T-splines: fundamentals and methods. *Comput. Methods Appl. Mech. Engrg.*, 316:349–372, 2017.

[58] P. Weinmüller and T. Takacs. Construction of approximate C^1 bases for isogeometric analysis on two-patch domains. *Comput. Methods Appl. Mech. Engrg.*, 385:114017, 2021.

[59] P. Weinmüller and T. Takacs. An approximate C^1 multi-patch space for isogeometric analysis with a comparison to Nitsche's method. Technical Report 2202.04516, arXiv.org, 2022.

[60] Q. Zhang, M. Sabin, and F. Cirak. Subdivision surfaces with isogeometric analysis adapted refinement weights. *Comput.-Aided Des.*, 102:104–114, 2018.